Master's thesis
Degree Programme in Materials Research
Computational Materials Research

LOCAL MODEL HAMILTONIAN CALCULATION OF RIXS AMPLITUDE OF Sr_3NiIrO_6

Levi Keller

16.09.2019

Supervisors: Simo Huotari
Keith Gilmore

Examiners: Simo Huotari
Kirsi Svedström

UNIVERSITY OF HELSINKI
FACULTY OF SCIENCE

P.O.Box 64 (Gustaf Hällströmin katu 2)
00014 University of Helsinki

HELSINGIN YLIOPISTO
HELSINGFORS UNIVERSITET
UNIVERSITY OF HELSINKI
MATEMAATTIS-LUONNONTIETEELLINEN TIEDEKUNTA
MATEMATISK-NATURVETENSKAPLIGA FAKULTETEN
FACULTY OF SCIENCE

Tiedekunta – Fakultet – Faculty	Koulutusohjelma – Utbildningsprogram – Degree programme
Physics	Master's Programme in Materials Research

Tekijä – Författare – Author

Levi Keller

Työn nimi – Arbetets titel – Title

Local model Hamiltonian calculation of RIXS amplitudes of Sr_3NiIrO_6

Työn laji – Arbetets art – Level	Aika – Datum – Month and year	Sivumäärä – Sidoantal – Number of pages
Master's Thesis	16.09.2019	44

Tiivistelmä – Referat – Abstract

The spin-orbit-coupled insulator Sr_3NiIrO_6 is a strongly correlated transition metal compound, where an interplay of geometric frustration and spin anisotropy gives rise to novel magnetic phases. Resonant inelastic x-ray scattering (RIXS) is a powerful probe of the low-lying quasi-particle excitations that underpin these emergent properties.

In this work, we partition the active space into approximately non-interacting parts in order to introduce a tight-binding single-particle model Hamiltonian describing the distorted IrO_6 octahedra in Sr_3NiIrO_6. We then use this model to calculate its RIXS spectrum at the Ir L3-edge in the sub-electronvolt range. The results of this calculation are compared with experiments performed at the European Synchrotron Radiation Facility, and with a multiplet crystal field model calculation.

We find that this one electron model largely agrees with the full-multiplet model and describes the d-d excitations observed in experiment. The addition of an exchange field term explains the low-lying temperature-dependent magnetic feature, disambiguating the sign of the crystal-field term, and suggesting that the feature is well localized at low temperatures, and is best described as an orbitally-entangled local spin-flip excitation. However, the correspondence at room temperature diminishes, suggesting that dispersive description is necessary to model this regime.

The drastic reduction in active space entailed by this model facilitates the creation of extended non-collinear Heisenberg-like models, which can be calculated at a lower computational cost than full multiplet extended models.

Avainsanat – Nyckelord – Keywords

Synchotron, Spectroscopy, Resonant Inelastic X-ray Scattering, model Hamiltonian, Spin-orbit coupling, Crystal Field

Säilytyspaikka – Förvaringställe – Where deposited

Helsinki University E-Thesis

Muita tietoja – Övriga uppgifter – Additional information

Contents

Introduction

Strongly correlated materials exhibit a very wide range of structural, electronic and magnetic properties, many of which are unusual and poorly understood. In strongly-correlated transition metal oxides (TMO), like the one treated in this work, much of this behavior emerges from the electronic structure of the open d-shell, and therein from the mutual influence of many varied effects, such as on-site Coulomb repulsion, Jahn-Teller distortion, orbital hybridization, ligand-field effects, spin-orbit coupling, and magnetic superexchange. The manner in which macroscopic properties emerge from the microscopic ones is an active area in condensed matter research, as study of how the observed phases of matter depend on these many-body effects can unveil experimental pathways to novel physical phenomena [1, 2].

Scattering experiments probe the electronic structure of materials, and of such methods Resonant Inelastic X-ray Scattering (RIXS) is one of the more versatile ones owing to its element, orbital and spin selectivity, and momentum resolution. This flexibility, however, complicates the interpretation of an experimental spectrum, which requires the deconvolution of a variety of effects.

One TM compound that has received much attention lately is the 5d TM oxide Sr_3NiIrO_6, which has aroused interest as a candidate for realizing a Kitaev spin-liquid [3, 4]. There has been some controversy as to the interpretation of its ground-state[5, 6, 7, 8, 9]. In this study we calculate its RIXS spectrum using a method based on the exact diagonalization of a single-particle model Hamiltonian. By comparing this result both to experiment and to a more general multiplet calculation, we gauge the descriptive power of the model and shed light on the ground state electronic structure of the compound and its relationship to emergent properties thereof.

In the sections 1-4, we lay the theoretical groundwork necessary to justify the construction of this model and the spectral computation that follows. In section 5, we review the literature on Sr_3NiIrO_6. The next section proceeds by describing in detail the computational methods employed. Finally we present the results and discuss their implications with respect to the literature on this topic.

Units and Symbols

In the theoretical background sections we use Hartree natural units:

$$e = \hbar = m_e = 1$$

where the speed of light is $c = \alpha^{-1} \approx 137$, and α is the fine structure constant. When presenting computational and experimental details, we revert to scale-appropriate SI derived units, such as electronvolts (eV) for energies.

1 Electronic structure

1.1 Introduction

The complete description of ordinary matter (consisting of electrons, photons, and nuclei with the internal structure of the latter neglected) and their interactions is the domain of quantum electrodynamics (QED). A single fermion is described by the Dirac Hamiltonian [10, 11]:

$$h_D = \beta mc^2 + c(\alpha \cdot \boldsymbol{p}) \tag{1}$$

where α and β are the Dirac matrices whose action is on a four component Dirac bispinor.

A system of n fermions is described by

$$H = \sum_{i=1}^{n} h_D(i) + \frac{1}{2} \sum_{i \neq j} g(i,j) \tag{2}$$

where $g(i,j)$ is the interaction between two fermions. A coarse approximation (exact in the nonrelativistic (NR) limit $c \to \infty$) yields the Coulomb interaction $g_0(i,j) = \frac{1}{r_{ij}}$. Replacing g with g_0 yields the Dirac-Coulomb Hamiltonian, the NR limit of yields the Levy-Leblond equation, which is a first order analogue to the Schrödinger equation (as the Dirac equation is to the Klein-Gordon equation):

$$\hat{\mathcal{H}}(\boldsymbol{\tau})\Psi(\boldsymbol{\tau}, t) = i\frac{\partial}{\partial t}\Psi(\boldsymbol{\tau}, t) \tag{3}$$

where $\boldsymbol{\tau} \equiv (\boldsymbol{\tau}_e, \boldsymbol{\tau}_n) \equiv (\boldsymbol{\tau_{e,1}}, ..., \boldsymbol{\tau_{e,n}}, \boldsymbol{\tau_{n,1}}, ..., \boldsymbol{\tau_{n,N}})$ are the spatial and spin coordinates of n electrons and N nuclei. Square-integrable (over $\boldsymbol{\tau}$) unit-norm solutions to this equation represent completely-determined (pure) bound states of the system. Free states are not square-integrable, and to avoid discussing the mathematical constructions necessary to properly treat them, we set box-normalized boundary conditions. The solutions to $\hat{\mathcal{H}}$ then span a separable complex Hilbert space $(\mathbf{H}_{\text{sys}}, \langle\cdot|\cdot\rangle)$. The Hamiltonian $\hat{\mathcal{H}}$ is an automorphism on $\mathbf{H}_{\text{sys}}$.

Since typical macroscopic systems contain $\sim 10^{23}$ particles, this is an inordinately complex equation, whose solution for any but the simplest of physical systems requires a series of successive approximations, many of which

are poorly controlled. The typical approach in condensed matter theory is to invoke any number of system-appropriate approximations that balance tractability and descriptive power, and which usually lead to the creation of model Hamiltonians over finite-dimensional Hilbert spaces, whose ultimate justification is experimental in nature. In this chapter, we outline the approximations made in this study and set up the formal language that will be employed in succeeding sections.

1.2 The Hamiltonian equation.

The Hamiltonian of a system with n electrons of N nuclei is

$$\hat{\mathcal{H}} = \hat{\mathcal{T}}_n + \hat{\mathcal{T}}_e + \hat{\mathcal{V}}_{nn} + \hat{\mathcal{V}}_{ne} + \hat{\mathcal{V}}_{ee} + \hat{\mathcal{H}}_{\text{rel}} \tag{4}$$

where

$$\hat{\mathcal{T}}_n = \sum_i^N \frac{\boldsymbol{\nabla}^2_{\mathbf{R}_i}}{2m_i} \qquad \hat{\mathcal{T}}_e = \sum_i^n \frac{\boldsymbol{\nabla}^2_{\mathbf{r}_i}}{2} \tag{5}$$

$$\hat{\mathcal{V}}_{nn} = \sum_{i<j}^N \frac{Z_i Z_j}{|\mathbf{R}_i - \mathbf{R}_j|} \qquad \hat{\mathcal{V}}_{ne} = \sum_i^n \sum_j^N \frac{-Z_j}{|\mathbf{r}_i - \mathbf{R}_j|} \tag{6}$$

$$\hat{\mathcal{V}}_{ee} = \sum_{i<j}^n \frac{1}{|\mathbf{r}_i - \mathbf{r}_j|} \tag{7}$$

and where, $\mathbf{r}_i(\mathbf{R}_i)$ are the spatial coordinates of the ith electron (nucleus), and $\hat{\mathcal{H}}_{\text{rel}}$ are relativistic effects obtained from the low-energy limit of the fully-relativistic Dirac equation [12]

$$\hat{\mathcal{H}}_{\text{rel}} = \alpha^2 \sum_{i=1}^n \frac{-\mathbf{p}_i^4}{8} - \frac{1}{4}\frac{\partial V}{\partial r_i}\frac{\partial}{\partial r_i} + \frac{1}{2r_i}\frac{\partial V}{\partial r_i}\mathbf{s}_i \cdot \mathbf{l}_i \tag{8}$$

where $\mathbf{s}_i$ and $\mathbf{l}_i$ are the spin and orbital angular momentum operators. $\mathbf{s}_i$ is an operator on the spinorial space, which is isomorphic to $\mathbb{C}^2$, and so even the single particle Schrödinger equation is actually a set of coupled complex-valued differential equations, or a 2x2 matrix equation. The only nonscalar term in the 1-particle matrix equation is the last term on the left-hand side of equation (8), which is known as spin-orbit coupling (SOC), and which therefore provides unique experimental pathways to probe the state of a system. Explicit treatment of nonscalar terms greatly increases the

computational complexity of the problem. Since, for hydrogenic orbitals, the SOC term scales as the fourth power of the effective nuclear charge Z_{eff}, it is often neglected for lighter elements [13, 12, 11].

With the exception of photons, which will be introduced later, the fundamental constituent particles at this level of theory are all spin-$1/2$ particles. These have a degree of freedom (often called internal) corresponding to the action of the fundamental representation of $\text{spin}(p,q)$, and coinciding with its double cover of the $\text{SO}(p,q)$ group. In nonrelativistic approximations, $p,q = 3,0$, and so the spin group is $\text{SU}(2)$. The action of $\text{SU}(2)$ on the active space $\mathbb{C}^2$ is given in the Pauli representation, which in the Cartesian basis of the frame bundle has generators

$$\mathbf{s} \equiv (s_x, s_y, s_z) \equiv \left(\begin{pmatrix} 0 & 1 \\ 1 & 0 \end{pmatrix}, i \begin{pmatrix} 0 & -1 \\ 1 & 0 \end{pmatrix}, \begin{pmatrix} 1 & 0 \\ 0 & -1 \end{pmatrix} \right)$$

associated with the $\text{SO}(3)$ generators $\mathbf{l} = (l_x, l_y, l_z)$ of rotations about the subscripted axes.

Using the isomorphism $L^2(\mathbb{R}^3 \otimes \mathbb{C}^{\not\in}) \simeq L^2(\mathbb{R}^3) \otimes L^2(\mathbb{R}^3)$ we describe this extra degree of freedom (dof) using basis functions $\chi_\pm : \{1,2\} \to \{0,1\}$

$$\begin{aligned} \chi_+ := \alpha(\sigma) : \qquad & \alpha(1) = 1 \qquad & \alpha(2) = 0 \\ \chi_- := \beta(\sigma) : \qquad & \beta(1) = 0 \qquad & \beta(2) = 1 \end{aligned}$$

so that every three spatial dofs correspond to one discrete valued variable σ, and the inner product on $\mathbf{H}_{\text{sys}}$ is that of $\bigotimes_{i=1}^{2n} L^2(\mathbb{R}^3)$.

As vectors, states have formal time dependence only, and we denote them using Dirac notation

$$\Psi(\boldsymbol{\tau}, t) \equiv |\Psi\rangle\,(t) \equiv |\Psi\rangle$$

We denote the natural dual vector of $|\Psi\rangle$ by $\langle\Psi|$, which is defined uniquely by the relation $\langle\Psi|\Psi'\rangle = \langle\Psi|\,(|\Psi'\rangle)$. Juxtaposition of vectors denotes tensor product, unless it is visually reminiscent of an inner product, in which case contraction in intended.

Although the distinction is largely semantic, we use Dirac notation to distinguish the abstract vector from a particular functional representation. To relate the two, one defines the dual vector $\langle \mathbf{x}, \mathbf{n}, t|$ for a system with discrete and continuous coordinates in $\mathcal{D}_d$ and $\mathcal{D}_c$ respectively by

$$\langle \mathbf{x}, \mathbf{n}|\,(|f\rangle) := \sum_{\mathbf{n}' \in \mathcal{D}_d} \int_{\mathcal{D}_c} \mathrm{d}\mathbf{x}' \delta^{\dim \mathcal{D}_c}(\mathbf{x} - \mathbf{x}') \delta_{\mathbf{n},\mathbf{n}'} f(\mathbf{x}', \mathbf{n}', t) = f(\mathbf{x}, t) \tag{9}$$

For (pure) states with a generic rather than function-denoting label, we write $\langle \mathbf{x}|\xi\rangle = \Psi_\xi(\mathbf{x}, t)$.

1.3 The Electronic Hamiltonian

The dynamic dependence on the spatial coordinates of the nuclei are suppressed by a factor of $m_\alpha^{-1} \sim 10^{-3}$. This forms the basis of the clamped-nuclei approximation, in which we treat the nuclear spatial coordinates as fixed parameters. We separate the Hamiltonian into a nuclear and electronic part, and apply the adiabatic approximation

$$\begin{aligned} \hat{\mathcal{H}} &= \hat{\mathcal{T}}_n + \hat{\mathcal{H}}_e \\ \Psi(\boldsymbol{\tau}, t) &= \Psi_e(\boldsymbol{\tau}_e, t; \boldsymbol{\tau}_n)\chi(\boldsymbol{\tau}_n) \end{aligned} \tag{10}$$

The nuclear coordinates are treated as parameters, and any dynamic dependence upon them is ignored. Nuclear dynamics can later be recovered by varying the spatial parameters to obtain the potential energy surface. This latter procedure is known as the Born-Oppenheimer approximation. In what follows, we restrict our attention to the electronic problem

$$\hat{\mathcal{H}}_e \Psi_e(\boldsymbol{\tau}_e, t; \boldsymbol{\tau}) = i\frac{\partial}{\partial t}\Psi_e(\boldsymbol{\tau}_e, t; \boldsymbol{\tau}) \tag{11}$$

and when the context is clear denote $\Psi_e(\boldsymbol{\tau}_e; \boldsymbol{\tau}_n, t)$ as simply $\Psi(\boldsymbol{\tau}_e, t)$, and $\hat{\mathcal{H}}_e(\boldsymbol{\tau}_e; \boldsymbol{\tau}_n)$ as $\hat{\mathcal{H}}(\boldsymbol{\tau}_e)$.

1.4 Stationary states

Solutions with a separable time dependence have a time dependent factor of e^{-iEt}. These are eigenvectors of the Hamiltonian, as $i\frac{\partial}{\partial t}\Psi = E\Psi = \hat{\mathcal{H}}\Psi$. Square-integrable separable solutions represent bound states, while unbound or continuum states are not square-integrable. To avoid unessential mathematical background, we describe our universe as a finite cubic region $\mathcal{D} \subset \mathcal{R}^3$ so the full spectrum of the Hamiltonian is discrete. One can select from these an orthonormal basis for a separable Hilbert space $\mathbf{H}_{\text{sys}} \simeq L^2(\mathcal{D}^n) \otimes \mathbb{C}^{2n}$. Solutions corresponding to physical states must have unit norm, and are therefore rays in $\mathbf{H}_{\text{sys}}$.

The existence of bound electron states implies that these must be described by a single electron wavefunction $\phi(\mathbf{r}, \sigma)$ [14]. Its dynamics are described by a single particle effective potential $\hat{\mathcal{V}}_{\text{eff}}$, such that ϕ is described by the Hamiltonian

$$\hat{\mathcal{H}}_{\text{MF}} = \frac{\boldsymbol{\nabla}^2}{2} + V_{\text{eff}}(\mathbf{r}, \sigma). \tag{12}$$

In many-body perturbative calculations, we write the Hamiltonian as

$$\sum_{i=1}^{n} \hat{\mathcal{H}}_{1\mathrm{e}}(\boldsymbol{\tau}_i) + \hat{\mathcal{H}}_{\boldsymbol{\tau}_\mathrm{e}} \tag{13}$$

and the exact solutions for either $\hat{\mathcal{H}}_{\mathrm{MF}}$ or H_{1e} are then used to form the tensor basis for $\hat{\mathcal{H}}_{\mathrm{sys}}$.

The spatial part of the single particle stationary states is called an orbital. The full eigenfunction, including Pauli spinors, is called a spin-orbital and its eigenvalue is the orbital ionization potential in the non-interacting limit. The span of all one-elecron (1e) states form the 1e Hilbert space $\mathbf{H}_1$. States with occupation n are built up from linear combinations of products of these 1e-wavefunctions:

$$\Psi(\boldsymbol{\tau}_1, \boldsymbol{\tau}_2, ..., \boldsymbol{\tau}_n) = \sum_{j=1}^{N} \prod_{i=1}^{n} \phi_{a_j}(\mathbf{r}_i)\chi(\sigma_i) \tag{14}$$

where ϕ_{a_j} is a 1e-wavefunction and χ is a spin function.

1.5 Antisymmetry

The spin-statistic theorem states that any physical state of n-fermions Ψ must be antisymmetric with respect to permutation of any two of its arguments, so $\bigotimes_{i=1}^{n} \mathbf{H}_1 \supsetneq \mathbf{H}_{\mathrm{sys}}$ for $n > 1$.

The antisymmetry requirement is satisfied by the Slater determinant

$$|\phi_1\chi_1, ..., \phi_n\chi_n| \equiv \frac{1}{\sqrt{n!}} \det \begin{vmatrix} \phi_1(\mathbf{r}_1)\chi_1(\sigma_1) & ... & \phi_1(r_n)\chi_1(\sigma_n) \\ \vdots & \ddots & \vdots \\ \phi_n(\mathbf{r}_1)\chi_n(\sigma_1) & ... & \phi_n(\mathbf{r}_n)\chi_n(\sigma_n) \end{vmatrix} \tag{15}$$

and the nonvanishing Slater determinants for n electrons, up to permutation of rows or columns, form a complete orthonormal basis of $\mathbf{H}_{\mathrm{sys}}$. We can directly replace the tensor product with the wedge product[1] of Slater-determinants:

$$|ab||cd| := |ab| \wedge |cd| = \frac{1}{2}|ab| \otimes |cd| - |cd| \otimes |ab|$$

[1] We conflate forms with their natural duals.

and adopting the notation for n-form subspaces Ω_n, we define the Fock space as $\mathcal{F} \equiv \Omega(\mathbf{H}_1) = \bigoplus_{i=1}^{\infty} \Omega_i(\mathbf{H}_1)$ and define the creation operator of an enumerated basis $a_i^\dagger \in \mathrm{End}(\mathcal{F})$ by

$$a_i^\dagger(|i_1...i_n|) := |i\rangle \wedge |i_1...i_n|$$

and the annihilation a_i as its hermitian conjugate.

1.6 Holes

For a subsystem of n electrons in an N-dimensional subspace, with $n > N/2$, it could be more convenient to describe a state by listing the unoccupied 1e states. In order to do this, we partition the 1-particle Hilbert space into finite-dimensional 'shells' or 'manifolds' with an ordered set of N basis functions $A = \mathrm{span}\{|a_i\rangle \, | i \in [1, N]\}$. This gives a canonical N-form $\omega \equiv |a_1, ..., a_N|$, with respect to which we define the hodge-star $* : \Omega^n(A) \to \Omega^{N-n}(A)$ implicitly via ($f \in \Omega(A)$)

$$|f| \wedge *|g| = \langle |f||g| \rangle \, \omega \tag{16}$$

Following Sugano [19] we call this operation adjugation, and within a shell, denote

$$|a_i^* a_j^*| \equiv *|a_i a_j|$$

but for two shells A and B we denote

$$|a_i^* b_j^*| \equiv *|a_i| \wedge *|b_j|$$

1.7 Symmetry

A symmetry with respect to some $\hat{\mathcal{H}} \in \mathrm{Aut}(\mathbf{H})$ is any operator $S \in \mathrm{Aut}(\mathbf{H})$ satisfying

$$| \langle S\phi | S\psi \rangle |^2 = | \langle \phi | \psi \rangle |^2 \tag{17}$$

$$S\hat{\mathcal{H}}S^{-1} = \hat{\mathcal{H}} \tag{18}$$

The set $G(\hat{\mathcal{H}})$ of all symmetry operators form a subgroup of $\mathrm{Aut}(\mathbf{H})$[13].

Wigner's theorem states that all symmetries of a quantum mechanical system must be either unitary and linear or antiunitary and antilinear. The latter are associated with a reversal of time, and do not concern us here[15].

For each eigenvalue λ in the spectrum $\sigma(\hat{\mathcal{H}})$, the set

$$\mathbf{H}_\lambda := \{|\phi\rangle \in \mathbf{H} | \hat{\mathcal{H}} |\phi\rangle = \lambda |\phi\rangle\}$$

forms a subspace of $\mathbf{H}$. We call this the degenerate subspace of λ, and we call $\dim \mathbf{H}_\lambda$ its degeneracy. We obtain the decomposition

$$\mathbf{H} = \bigoplus_{\lambda \in \sigma(\mathbf{H})} \mathbf{H}_\lambda$$

which is a partition of the Hilbert space into the aforementioned shells. By choosing an *orthonormal* basis $\{\phi_{\lambda,i} | i \in [1, \dim(\mathbf{H}_\lambda)]\}$ for a degenerate subspace, we can directly identify $G(\hat{\mathcal{H}}_\lambda) = G(\hat{\mathcal{H}})\Big|_{\mathbf{H}_\lambda}$ with a *unitary* irreducible representation (irrep) $D^{(\lambda)}$ of symmetry group $G(\hat{\mathcal{H}})$: $D^{(\lambda)} : G \to \mathbb{C}^{\dim(\mathbf{H}_\lambda)^2}$ defined elementwise by

$$D^{(\lambda)}(g)_{\alpha,\beta} := \langle \phi_{\lambda,\alpha} | g | \phi_{\lambda,\beta} \rangle$$

The basis vectors are called partners of the irreps. We label state by irrep Γ (identified up to unitary equivalence), partner γ and an additional (multi)index α to account for the multiple occurrences of Γ.

The symmetry group of a multiparticle system described by $\hat{\mathcal{H}} = \sum_{i=1}^n \hat{\mathcal{H}}_1(\tau_i)$ is $\bigotimes_{i=1}^n G(\hat{\mathcal{H}}_1)$. However, in the case of coordinate transformations, we retain only the diagonal subgroup $\{\bigotimes_{i=1}^n g | g \in G_S(\hat{\mathcal{H}}_1)\} \cong G(\hat{\mathcal{H}}_1)$, with which the interaction term also commutes. Given any particular representation $D^{(\Gamma)}$ of a group action on the 1-particle Hilbert space, a natural representation for the action on the 2-particle Hilbert space is given by the Kronecker product $D \otimes D$, whose reduction to irreps is given by a unitary matrix whose elements are called Clebsch-Gordan (CG) coefficients

$$C^{\alpha\Gamma\gamma}_{\alpha_1\Gamma_1\gamma_1 \ldots \alpha_n\Gamma_n\gamma_n} = (\langle \alpha_1\Gamma_1\gamma_1| \otimes \ldots \otimes \langle \alpha_n\Gamma_n, \Gamma_n|) |\alpha\Gamma\gamma\rangle \tag{19}$$

1.8 Reduction of symmetry

The full symmetry group of a physical system is the double cover of the Poincare group, defined via their action in coordinate space. As noted above, we restrict our consideration to the unitary subgroup $\mathbb{R}^3 \rtimes SU(2)$, and when applying the clamped nuclei approximation, or in the presence of an external potential, a further reduction occurs. A common symmetry reduction occurs

when a perturbation lowers the symmetry of the system. In this case we can relate the generically refined partition of $\mathbf{H}$ under the reduced symmetry group to the coarser unperturbed partition via the great orthogonality theorems of representation theory[16].

Two such preperturbative partitions are of key importance in condensed matter theory: the first is obtained by restriction to SO(3) (neglecting SOC) or SU(2). The representation theory of these groups is well known, and the $2j+1$-dimensional irreps of SU(2) are labeled by whole or half integer j, with integer j are also irreps of SO(3), while partners are labeled by whole or half integer m_j ranging from $-j$ to j in integer steps. At the coordinate level, this implies separability of the differential equation into radial and angular parts. Solutions (wavefunctions) can also then be factored into radial and angular parts. The radial part is a one-dimensional Hamiltonian which depends only on the irrep, and is therefore indexed by n and j. The angular part depends on irrep and partner, and is therefore indexed by j and m. Where we take the spin to be separable, j is restricted to whole integers, and we typically distinguish it with the generic label l. Spectroscopists use the letter sequence $s, p, d, f, g, h...$ corresponding to $l = 0, 1, 2, 3...$

The second is the finite translation group $\mathcal{T} \simeq \mathbb{Z}_N^d$, for a d-dimensional crystal, where N is generally taken to be arbitrarily large. This is commutative, and hence by Burnside's theorem must have as many irreps as elements, so each irrep is 1-dimensional. and therefore have the form $e^{i\theta(g)}$. Since $g \in \mathbb{Z}_N \implies g^N = e$, N successive application of the irrep must be equivalent to multiplication by 1, which means that $e^{i\theta(g)N} = 1 \implies \theta(1)N = m2\pi \implies \theta(1) = \frac{m2\pi}{N}$. For the irrep to be faithful, it must be generated by some m, which can be unique for only N different values of m so each set of d generators uniquely corresponds to an irrep. The requirement that any state transform as an irrep of $\mathcal{T}$ is known as Bloch's theorem, which is usually stated in the form

$$\phi(\mathbf{r}) = e^{i\mathbf{k}(g_1 \otimes g_2 \otimes g_3)\cdot\mathbf{r}} u(\mathbf{r}) \tag{20}$$

where $u(\mathbf{r})$ has the full symmetry of the crystal, and $k_i = \frac{2\pi m_i}{n_i a_i}$ corresponds to an irrep of $\mathcal{T}$, and is known as crystal momentum. We can therefore describe single-electron Bloch states as

$$\phi_{n,k} = u_{n,\mathbf{k}}(r) e^{i\mathbf{k}\cdot r} \tag{21}$$

where the index n accounts for multiplicity of the irrep $\mathbf{k}$. The nonredundant set of $\mathbf{k}$-values nearest $\mathbf{k} = 0$ is called the first Brillouin zone (FBZ).

2 Model Hamiltonians

In this section, we describe general approaches for reducing the complexity of the formalism thus far developed. These simplifications lead to model Hamiltonians that can describe pertinent features of a physical system with a small number of parameters that can be related to experiment.

2.1 Mean field theory and correlation

Mean field theories (MFT) attempt to estimate $\hat{\mathcal{V}}_{\text{eff}}$, in the hope that the many-particle Hamiltonian is principally diagonal in the basis given by the ensuing Slater determinants. This is the case when the electrons are weakly correlated. Two 1e states are uncorrelated if the probability of simultaneously finding one at position $\mathbf{r}_1$ and another at position $\mathbf{r}_2$ is equal the product of the two independent probabilities. In Hartree-Fock MFT, one distinguishes between correlation and electron exchange effects, where the latter arise as the exchange integral of two electron operators, ie, the last term on the LHS of

$$\langle |ab||\mathcal{O}||ab| \rangle = \langle ab|\mathcal{O}|ab\rangle - \langle ab|\mathcal{O}|ba\rangle \,, \tag{22}$$

where the first term is called the direct 2e-integral. Exchange effects are also called Fermi correlation, because they can be related to the Fermi-hole in Thomas-Fermi MFT, which can be understood as the Pauli exclusion of electrons of like spin. Since this tends to decrease the Coulomb repulsion, it leads to a lowering of energy for spin aligned wavefunctions vis-a-vis those with opposing spin. It is therefore related to Hund's coupling parameter J_H which describes precisely this effect[17]. Correlation may therefore refer to the difference between the Hartree-Fock limit and the exact solution.

2.2 Tight binding

In the tight binding picture, we partition $\sigma(\hat{\mathcal{H}}_{1\text{e}})$ into quasi-continuous bands $E_n(\mathbf{k})$ which can be related to atomic orbitals that collectively contribute to them. This can be justified by treating the non-co-centric electron-electron interaction and lattice potential (with the removal of one center) as a perturbation of the isolated atom, in which case atomic SU(2) symmetry is reduced to a finite subgroup, and translational symmetry is introduced. Where the overlap of atomic orbitals is minimal, the dispersion is nominal: $E_n(\mathbf{k}) \approxeq E_n(0)$, and we can speak of low-dispersion (flat) bands of tightly-bound electrons. Electrons in these bands are sometimes called 'localized',

although true localization is only possible in completely flat bands, which in a perfect crystal can only be realized as a limit, and the term should more properly be reserved for states bound to impurities.

In the tight-binding approximation, we consider an orthonormal set of localized orbitals centered on nuclear sites at $\mathbf{R}$ as provided by the Wannier functions

$$\mathfrak{w}_{n,\mathbf{R}}(\mathbf{r}) = \frac{1}{\sqrt{N}} \sum_{\mathbf{k}} e^{-i(\mathbf{k}\cdot\mathbf{R}+\phi(\mathbf{k}))} \psi_{n,\mathbf{k}}(\mathbf{r}) \tag{23}$$

where $\psi_{n,\mathbf{k}}(\mathbf{r})$ are the Bloch functions of eq. (21), the summation over $\mathbf{k}$ is over k-points in the first Brillouin zone, and $\phi(\mathbf{k})$ is an arbitrary real-valued function, usually optimized so as to maximize the orbital's localization.

When localization is attainable and the resulting Hamiltonian is principally diagonal, a model for a lattice built of a single atomic species, with a single electron in its open shell, neglecting 2nd and higher nearest neighbor interactions can be reduced to just two parameters: the onsite Coulomb repulsion

$$U := \int \mathrm{d}\mathbf{r}\mathrm{d}\mathbf{r}' \; \hat{\mathcal{V}}(\mathbf{r},\mathbf{r}') \; \mathfrak{w}^*_{\mathbf{R}}(\mathbf{r})\mathfrak{w}^*_{\mathbf{R}}(\mathbf{r}')\mathfrak{w}_{\mathbf{R}}(\mathbf{r})\mathfrak{w}_{\mathbf{R}}(\mathbf{r}')$$

also called the Hubbard-U, and the hopping integral

$$t := \int \mathrm{d}\mathbf{r}\mathcal{T}_e(\mathbf{r})\mathfrak{w}^*_{\mathbf{R}}(\mathbf{r})\mathfrak{w}_{\mathbf{R}'}(\mathbf{r})$$

Model Hamiltonian based on these and other derived parameters are employed to describe highly correlated materials which defy the predictions of MFTs. These models, typically written in second quantization formalism, restore the many-body nature of the underlying equations in the critical region near the Fermi level, while relying on the simplifications of the tight-binding approximation to elide much of the description. The Hubbard model describes a singe spin degenerate band with local orbital basis indexed by lattice site and spin

$$\hat{\mathcal{H}} = -t \sum_{i,j\in A_i,\sigma} a^\dagger_{i\sigma} a^\dagger_{j\sigma} + U \sum_i n_{i+} n_{i-} \tag{24}$$

where A_i is the set sites neighboring i, and $n_{i\sigma} = a^\dagger_{i\sigma} a_{i\sigma}$ is the number operator. The Hubbard model has been solved exactly for one dimensional systems (linear chains) and for the limit of infinite dimensions, but analytical solutions for three dimensional systems are not available and mean field approaches are required. Where U exceeds the bandwidth of a partially filled

band, a band gap opens up, and a nominal conductor becomes insulating. These Mott-Hubbard insulators are the prototypical correlated compounds, because they have been extensively studied, and key features arising from them, are regularly fed parametrically back into MFTs in an effort to explain correlated phenomena.

The Heisenberg model takes a statistical approach, accounting for both a mean field operator h and a coupling constants $J \propto t^2/U$ arising from an isotropic exchange interaction. The effects captured by these parameters underlie the magnetic behavior of many systems. The Heisenberg Hamiltonian is

$$\hat{\mathcal{H}} = -\frac{J}{2} \sum_{i,j \in A_i} \mathbf{s}_i \cdot \mathbf{s}_j - \sum_i h s_j.$$

More general models account for anisotropic exchange and nonparallel coupling of neighboring sites. Antisymmetric exchange, known as Dzyaloshinski-Moriya interaction, arises from relativistic SOC effects [18, 3].

2.3 Crystal field theory

Within the tight binding picture, crystal field theory describes systems in which the full rotational symmetry of hydrogenic orbitals is reduced by a perturbative crystal field $\hat{\mathcal{V}}_n$ to a finite subgroup. The effective potential can be expanded as [19]

$$V(r, \phi, \theta) = \sum_{k=0}^{\infty} \sum_{m=-l}^{l} a_{k,m}(r) Y_{k,m}(\phi, \theta) \tag{25}$$

In the spherical basis $\{|nlm\rangle\}$, the operator is given as

$$V = \sum_{\substack{n_1,n_2 \\ k,l_1,l_2 \\ m_1,m_2,m}} \langle n_1 l_1 m_1 | V(r, \phi, \theta) | n_2 l_2 m_2 \rangle \tag{26}$$

$$= \sum_{\substack{n_1,n_2 \\ k,l_1,l_2 \\ m_1,m_2,m}} \langle l_1 m_1 | Y_{k,m} | l_2 m_2 \rangle \int_0^{\infty} R^*_{n_1,l_1}(r) R_{n_2,l_2} a_{k,m}(r) \tag{27}$$

where $|n_i, l_i\rangle$ refers to the radial part of the ith orbital, $|l_i, m_i\rangle$ to the angular part, and $a_{k,m} \equiv 0$ when $|m| > k$.

The matrix element

$$\begin{aligned}
&\langle l_1 m_1 | l_2 m_2 | l_3 m_3 \rangle \\
&= \int_0^{\pi} \mathrm{d}\theta \int_0^{2\pi} \mathrm{d}\phi Y_{l_1,m_1}(\theta,\phi) Y_{l_2,m_2}(\theta,\phi) Y_{l_3,m_3}(\theta,\phi) \\
=&\sqrt{\frac{(2l_1+1)(2l_2+1)(2l_3+1)}{4\pi}} \begin{pmatrix} l_1 & l_2 & l_3 \\ 0 & 0 & 0 \end{pmatrix} \begin{pmatrix} l_1 & l_2 & l_3 \\ m_1 & m_2 & m_3 \end{pmatrix}
\end{aligned} \tag{28}$$

where

$$\begin{pmatrix} l_1 & l_2 & l_3 \\ m_1 & m_2 & m_3 \end{pmatrix} := \frac{(-1)^{l_1 - l_2 - m_3}}{\sqrt{2l_3+1}} \langle l_1, m_1; l_2, m_2 | l_3, -m_3 \rangle$$

are the Wigner 3j-symbols, which are defined in terms of the Wigner coefficients, is subject to selection rules that reduce the infinite sum to a small number of nonzero terms that can be related to each other by ensuring that $V(r, \theta, \phi)$ respects the local symmetry.

The single electron states can be classified by irrep in the manner described in the preceding sections. We describe the valence shell with a model Hamiltonian with this potential, usually parametrized in terms of the intrashell splitting of single electron energy states. After removing the centrosymmetric part (which corresponds to an arbitrary shift of the energy scale), we call this the crystal field potential. When the valence shell splits into two levels, we can unambiguously call this splitting parameter the crystal-field strength.

We can then introduce the intrashell Coulomb interaction as a perturbation. These are usually expanded in terms of the spherical harmonics as

$$\frac{1}{r_{12}} = \sum_{k=0}^{\infty} \sum_{l=-k}^{k} \frac{r_<^k}{r_>^{k+1}} Y_{k,m}^*(\theta_1, \phi_1) Y_{k,m}(\theta_2, \phi_2) \tag{29}$$

where $r_<(r_>) \equiv$min (max) $\{r_1, r_2\}$, we can separate out the angular integrals.

The diagonal matrix elements corresponding to atomic orbitals n_1, l_1, n_2, l_2 yield direct and exchange radial integrals, which are call the Slater-Condon parameters, and are given by the symbols

$$F^k_{n_1l_1n_2l_2} \equiv \int_0^\infty \mathrm{d}r_1 \int_0^\infty \mathrm{d}r_2 R^*_{n_1l_1}(r_1) R^*_{n_2l_2}(r_2) r^k_< r^{-k-1}_> R_{n_1l_1}(r_1) R_{n_2l_2}(r_2)$$
$$G^k_{n_1l_1n_2l_2} \equiv \int_0^\infty \mathrm{d}r_1 \int_0^\infty \mathrm{d}r_2 R^*_{n_1l_1}(r_1) R^*_{n_2l_2}(r_2) r^k_< r^{-k-1}_> R_{n_1l_1}(r_2) R_{n_2l_2}(r_1) \tag{30}$$

When clear from context, we drop reference to indices n_i, and use spectroscopic notation $k = 0, p = 1, d = 2...$ for indices l_i.

3 The RIXS cross-section

3.1 Introduction

Resonant inelastic X-ray scattering (RIXS) is a photon-in photon-out spectroscopy where energy of the incoming photon is tuned to the resonance excitation energy of a core electron. RIXS is a coherent 2nd order process, which means that the system can be described as passing through all possible virtual intermediate states where the adjective 'virtual' denotes that it may differ in energy from the initial and final state energy. In other words, energy is not conserved in the intermediate state. The experimental outcome is given by the weighted sum over intermediate states, with a weight proportional to the deviation from energy conservation. This would imply a singular contribution from the intermediate state that does conserve energy, but the singularity is convoluted with a bounded distribution owing to the Heisenberg uncertainty principle. By tuning the incident photon energy so that the initial state (consisting of the target ground state and noninteracting incoming photon) coincides with some given (photon free) intermediate state[2], one obtains the resonance condition, wherein the contribution of a particular degenerate level dominates the experimental outcome, affording a unique clarity of signal interpretation. Utilizing the x-ray portion of the spectrum allows one to tune into tightly-bound core electrons. This makes the probe sensitive to a particular atomic species (and site, if well-separated), and fixes the allowed symmetries of the initial and final states by means of the selection rules governing transitions (ie. matrix elements of the type implicated in the radiation process)[20].

Even with the resonant amplification, however, the cross-section is quite low, and most experiments are performed at synchrotron-radiation facilities, where sufficiently intense radiation is available to obtain a statistically significant number of scattering events in a short timespan. Radiation at these facilities is naturally polarized and coherent, and this enables exploitation of the spin and orbital selectivity of the RIXS process[21, p. 377]. Variation in detector positioning and sample orientation afford access to a wide range of momentum transfers.

[2]This is the usual setup. If the target is kept in an excited state during the experiment, for example by lasing, then an intermediate state with two photons could also be resonant.

3.2 Cross-section

A perturbative description of the interaction of matter with radiation is obtained via minimal substitution [14, p. 228]

$$p^\mu \to p^\mu - qA^\mu \tag{31}$$

where $p^\mu = (E, \mathbf{p})$ is the 4-momentum and $A^\mu = (\phi, \mathbf{A})$ is the electromagnetic 4-potential.

In box-normalized operator form, the electromagnetic vector potential is

$$\mathbf{A}(\mathbf{r}) = \sum_{\mathbf{k},\boldsymbol{\varepsilon}} \sqrt{\frac{2\pi}{V|\mathbf{k}|}} \left(\boldsymbol{\varepsilon} a_{\mathbf{k}\boldsymbol{\varepsilon}} e^{i\mathbf{k}\cdot\mathbf{r}} + \boldsymbol{\varepsilon}^* a^\dagger_{\mathbf{k}\boldsymbol{\varepsilon}} e^{-i\mathbf{k}\cdot\mathbf{r}} \right) \tag{32}$$

where $\mathbf{a}_{\mathbf{k}\boldsymbol{\varepsilon}}, (\mathbf{a}^\dagger_{\mathbf{k}\boldsymbol{\varepsilon}})$ is the bosonic annihilation (creation operator), $\boldsymbol{\varepsilon}$ is one of the two mutually orthogonal unit vectors orthogonal to $\mathbf{k}$, and k takes on all values allowed by the boundary conditions, namely $k_i = \frac{2\pi n_i}{\sqrt[3]{V}}$ for some integer n_i.

The condition $\mathbf{k} \perp \boldsymbol{\varepsilon}$ leaves two degrees of freedom in choosing a polarization basis. In a right-handed Cartesian basis whose third component is in the direction of $\mathbf{k}$ we define the circularly polarized components as

$$\boldsymbol{\varepsilon}_\pm = \mp \frac{1}{\sqrt{2}} \begin{pmatrix} 1 \\ \pm i \\ 0 \end{pmatrix} =: |\pm\rangle \tag{33}$$

which have the convenient properties of a) transforming under rotations like a rank 1 spherical tensor and b) being orthogonal to its complex conjugate.

Under minimal substitution, the electronic Hamiltonian is

$$\begin{aligned} \hat{\mathcal{H}}_e = \sum_{i=1}^{n} \frac{(\mathbf{p}_i + \mathbf{A}(\mathbf{r}_i))^2}{2} - \frac{1}{2}\boldsymbol{\sigma}_i \cdot (\mathbf{B}(\mathbf{r}_i)) + \sum_{j \neq i} \frac{1}{|\mathbf{r}_i - \mathbf{r}_j|} \\ + \frac{1}{4}\boldsymbol{\sigma}_i \cdot (\mathbf{E}(r) \times (\mathbf{p}_i + \mathbf{A}(\mathbf{r}_i))) \sum_{\mathbf{k}\boldsymbol{\lambda}} a^\dagger_{\mathbf{k}\boldsymbol{\varepsilon}} a_{\mathbf{k}\boldsymbol{\varepsilon}} \end{aligned} \tag{34}$$

We split off $\hat{\mathcal{H}}_{\mathrm{EM}}$ containing the terms involving vector potential $\mathbf{A}$ for a perturbative treatment and recover the Hamiltonian of eq. (7) with additional diagonal terms that account for the energy of non-interacting photons.

The differential cross section $\frac{\mathrm{d}\sigma}{\mathrm{d}\Omega}$ is the probability distribution, per unit time and per incident flux, of detecting a scattered particle in the solid angular

region $d\Omega$ far enough from the scatterer so that the interaction between the scattered particle and the scatterer can be neglected. It is given by Fermi's golden rule (to second order) as

$$\mathfrak{w} = 2\pi|\mathcal{M}_{\mathbf{fi}}|^2\delta(E_f - E_i) \tag{35}$$

$$\mathcal{M}_{\mathbf{fi}} = \langle\mathbf{f}|\hat{\mathcal{H}}_{\mathrm{EM}}|\mathbf{i}\rangle + \sum_n \frac{\langle\mathbf{f}|\hat{\mathcal{H}}_{\mathrm{EM}}|\mathbf{n}\rangle\ \langle\mathbf{n}|\hat{\mathcal{H}}_{\mathrm{EM}}|\mathbf{i}\rangle}{E_i - E_n + i\epsilon} \tag{36}$$

where $\mathbf{i}, \mathbf{n}$, and $\mathbf{f}$ respectively label initial, intermediate, and final states of the combined noninteracting system, and

$$\hat{\mathcal{H}}_{\mathrm{EM}} = \sum_i \frac{1}{2}\mathbf{A}(\mathbf{r_i})^2 + \mathbf{p}_i \cdot \mathbf{A}(\mathbf{r}_i) + \hat{\mathcal{H}}_{\mathrm{EM},1} \tag{37}$$

where $\hat{\mathcal{H}}_{\mathrm{EM,q}}$ indicates higher order terms with respect to the dipole expansion parameter, which will be discussed later.

The ϵ in the denominator is a formal parameter understood as limiting to zero after the limit of non-interaction is attained (ie. after the time/distance of the scatterer from the system is increased arbitrarily on either temporal side of the scattering process). In scattering experiments on macroscopic systems, it is replaced with a factor Γ (or $\Gamma/2$), called the lifetime energy, which accounts for the energy-time uncertainty in the denominator, and gives a Lorentzian profile to the divergence. This effect, called intrinsic lifetime broadening, is convoluted with instrumentation broadening, whose profile depends on the experimental setup, and statistical or band broadening of approximately degenerate states.

3.3 RIXS cross section

In the RIXS process, we have a transition

$$|\mathbf{i}\rangle = |i\rangle\,|\mathbf{k}_i, \boldsymbol{\varepsilon}_i\rangle \to |\mathbf{f}\rangle = |f\rangle\,|\mathbf{k}_f, \boldsymbol{\varepsilon}_f\rangle$$

where $|\mathbf{k}, \mathbf{p}\rangle$ is the state containing a photon labeled by its wave vector and polarization, and $|f\rangle, |i\rangle$ are the noninteracting final and initial state respectively. The amplitude $\mathcal{M}_{\mathbf{fi}}$ can be split into a first order term proportional to $\mathbf{A}^2$ and a second order term containing the operator $\mathbf{A}\cdot\mathbf{p}$ twice. The former, governed by the operator $\boldsymbol{\varepsilon}_o^* \cdot \boldsymbol{\varepsilon}_i e^{i(\mathbf{k}_o - \mathbf{k}_i)\cdot\mathbf{r}}$, is implicated in diffraction experiments, and usually suppressed by an appropriate choice of experimental geometry. The latter can be split into two terms, one with an intermediate

state photon, and one without. Higher order terms, containing any number of intermediate state photons, are not considered here. Using the commutation relation $i\mathbf{p} = [\hat{\mathcal{H}}, \mathbf{r}]$ we obtain the result for the double differential cross section

$$\frac{\partial^2 w}{\partial\Omega\partial\omega} \propto \frac{\omega_o}{\omega_i}\left|\sum_{|n\rangle\in\mathbf{H}_i}\langle f|\left(\boldsymbol{\varepsilon_o}\cdot\boldsymbol{\varepsilon_i}e^{i(\mathbf{k}_i-\mathbf{k}_o)\cdot\mathbf{r}}+\right.\right. \tag{38}$$
$$\left.\left.\frac{\mathcal{T}^\dagger(\mathbf{k_o},\boldsymbol{\varepsilon_o})\,|\mathbf{n}\rangle\,\langle\mathbf{n}|\,\mathcal{T}(\mathbf{k_i},\boldsymbol{\varepsilon_i})}{E_i-E_n+\omega_i-i\epsilon}+\frac{\mathcal{T}^\dagger(\mathbf{k_i},\boldsymbol{\varepsilon_i})\,|\mathbf{n}\rangle\,\langle\mathbf{n}|\,\mathcal{T}^\dagger(\mathbf{k_o},\boldsymbol{\varepsilon_o})}{E_i-E_n+k_o-i\epsilon}\right)|i\rangle\right|^2$$

where

$$\mathcal{T}(\mathbf{k},\boldsymbol{\varepsilon}) = \sum_i \mathbf{r}_i\cdot\boldsymbol{\varepsilon}e^{i\mathbf{k}\cdot\mathbf{r}_i} \tag{39}$$

In the dipole approximation, we assume that $\mathbf{k}\cdot\mathbf{r}_i << 1$ over the most significant part of its domain, and neglect the exponential term entirely. This is valid when the wavelength of incident radiation far exceeds the Bohr radius, and is somewhat coarse for the hard X-ray range. Inclusion of the first order term in the exponent series expansion, which contains a term $\mathbf{r}_i\cdot\boldsymbol{\varepsilon}\mathbf{k}\cdot\mathbf{r}_i$ is only consistent upon simultaneous inclusion of the magnetic term in $\hat{\mathcal{H}}_{\mathrm{EM}}$.

The elastic contribution is typically suppressed by an appropriate choice of scattering geometry, and the resonant condition ensures that the second term in equation (38) dominates the spectrum.

4 The RIXS spectrum (elementary excitations)

An excitation is a deviation of a system from its ground state. Since the response properties of a system depend upon its excited states, they determine its macroscopic properties. Single particle excitations, which can largely be ascribed to a change in the occupation of a single orbital eigenstate of the effective single particle Hamiltonian, is often distinguished from collective excitations, which are attributable to a small change in many orbital occupations or other degrees of freedom. For example phonons are a collective correlated small change in the degrees of freedom of the lattice potential.

It is often the case that an excited state which differs in energy from the ground state by $\Delta E = E_e - E_g$ can be described as the sum of two smaller excitations $\Delta E \approxeq \Delta E_1 + \Delta E_2$. This forms the basis for quasiparticle formalism, in which we term the excitations that do not admit such a decomposition

elementary, and describe them as quasiparticles in a Fock space, which are created or destroyed during the transitions, and ascribe the energy difference $E_i = \Delta E - \Delta E_1 + \Delta E_2$ to an interaction between the two quasiparticles. This allows us to write an effective Hamiltonian using second quantization formalism, in which we factor out the ground state (shifting the energy scale by E_g).

The single-electron hole states described previously are both quasiparticles and are describable in the single particle picture. In a result termed the orthogonality catastrophe, [22] showed that the states of the new system will be orthogonal to those of the old. Using the sudden approximation, we see that the excitation of a single hole leaves a macroscopic system with $\sim 10^{23}$ electron-hole pairs. The primacy of this description has been verified in experiment [23].

More formally, we can describe excitations as arising from the various degrees of freedom of the system, and the elementary excitations as those in which the system gains energy in a particular degree. Strongly correlated systems are then those in which the degrees of freedom are highly entangled.

The macroscopic properties of materials depend critically on their elementary excitations, since they are implicated in their response to external stimuli. In strongly correlated materials, these are poorly understood, and it is precisely in such materials that many unusual emergent properties can be found.

5 Sr_3NiIrO_6

5.1 Introduction

Transition metal oxides (TMOs) are a class of crystalline compounds in which transition metals cations are surrounded by oxygen ligands (cages), which determine the local symmetry character of the open $d-$ shell, most commonly octahedral (O_h) or tetrahedral (T_d), subordinate to the global rotational and translational symmetries of the crystal. These cages may share all their faces, but in many interesting compounds they are embedded in a host matrix of magnetically inactive cations, typically alkaline earth metals like calcium, strontium or barium, which affect the emergent magnetic and electronic properties primarily via their structural role. The TM cages may be edge, face or corner sharing, forming planar substructures, as is typical of the high-T superconductors, or linear chains, which lend themselves well to analysis by Heisenberg-like models.

Among the most intensively studied TMOs are the two-dimensional perovskites ($A^{2+}B^{4+}C_3^{2-}$) that comprise the parent compounds of the high-T_C superconductors. The superconducting behavior can be lifted by applying a strong external magnetic field to reveal a rich phase diagram, with both short range and long range correlated regimes, including antiferromagnetism, strange metal, charge density wave and pseudogap phases [24]. Perovskite solar cells have recently attained efficiencies approaching those of silicon cells, and this has been driven by research into the interrelation between electronic and macroscopic properties, which guides experimentalists in tuning the spectral response properties that play a critical role in efficiency [25].

As they scale strongly with effective atomic number, SOC effects become more pronounced in the higher periods of the periodic table. Counterparts to the 2d cuprates, such as Sr_2IrO_4, have attracted attention as an indirect means of studying superconductivity. The discovery in 2008 of an SOC-induced Mott-state, however, has drawn attention to the iridates in their own right. The effects of SOC on highly correlated systems introduces anisotropic spin interactions, introducing frustration to otherwise isotropic systems. The Kitaev model of a frustrated magnetic order on a honeycomb lattice, in particular, has spurred research into canditates like Sr_3NiIrO_6[2, 1]. Such compounds are particularly relevant to the nascent field of spintronics.

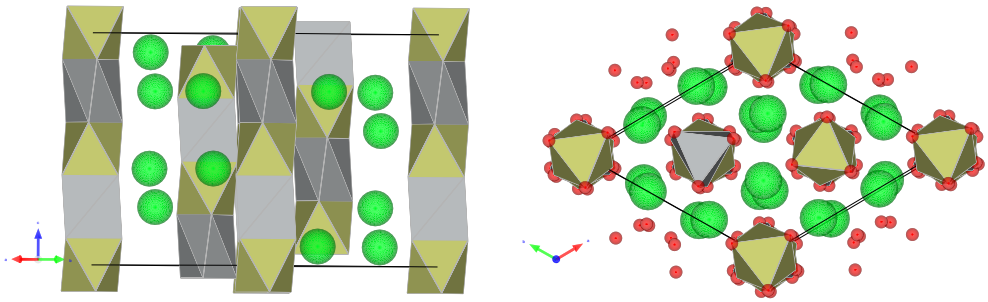

Figure 1: Unit cell of Sr_3NiIrO_6. Strontium positions are indicated with green spheres, nickel-centered octahedra in silver and iridium-centered distorted octahedra are gold. Each vertice is centered on an oxygen site, which are shown as red spheres in the view along the c-axis (right). Produced with Vesta[26].

5.2 Structure and Magnetic Properties

Sr_3NiIrO_6 belongs to the class $A_3MM'O_6$ TMOs, which is closely related to the double perovskites ($A_2MM'O_6$), and which consists of collinear chains of alternating MO_6 polyhedra and $M'O_6$ trigonal prisms, with adjacent polyhedra sharing a triangular face or edge along the c-axis. The overall spacegroup symmetry (up to magnetic orientation) of $Sr_3NiIrO_6$is $R\bar{3}c$, with direct structure parameters a = 9.58 Å and c = 11.13 Å (figure 1). Trigonal prisms are distorted octahedra, and the local symmetry group reduction, from O_h to $D3_d$, splits the M' t_{2g} level into a_1 and $(t_{2g})e_g$ (figure 2) with the distinct possibility of $(t_{2g})e_g$ - $(e_g)e_g$ mixing. Both polyhedra alterate in orientation such that a translation of half a unit cell along the c-axis corresponds to a 60° rotation about the same axis. The chains themselves are separated by buffering regions of alkaline earth metal cations A^{2+}, and like polyhedra in neighboring chains are staggered in position along the c-axis, allowing a corkscrew-like simultaneous translation and rotation about that axis. While the linear structure lends itself well to either ferromagnetic (FM) or antiferromagnetic (AF) global order, any magnetic ordering in the perpendicular plane is geometrically frustated, paving the way for a quantum liquid phase[27].

Many structures in this class exhibit a partially disordered antiferromagnetic (PDA) phase between two critical temperatures. The signature of this PDA phase is a slow spin-dynamic [28]. The PDA phase yields to a glass-like frozen disordered state upon cooling past the lower critical temperature, and susceptibility decreases drastically. In the presence of an external field, how-

ever, the susceptibility rises to a maximal value, as the magnetic order is frozen-in [29].

$Sr_3NiIrO_6$was first synthesized by Nguyen et al. [30] in a systematic study of the effect of fixing the M' = Ir^{4+} ionic centers, which have a single vacancy in their open t_{2g}-shell, while varying the electronegativity of the cation M. On the basis of susceptibility studies, they suggest a transition from AF ordering at a bit under 20 K to ferromagnetic (FM) ordering at higher temperatures, and rule out structural changes at this transition temperature.

Flahaut et al. [28] undertook a more detailed study of its magnetic properties, and calculated from the susceptibility curve an effective magnetic moment consistent with a low-spin configuration at the Ir^{4+} site (d^5, S = ½), and a high-spin configuration at the Ni^{2+} site (d^8, S = 1). They found a negative Curie-Weiss temperature, indicating that AF fluctuations dominate at high temperatures, giving overall ferrimagnetism along the chains. This is further indicated by absence of saturation in fields of to 35 T. At critical onset temperature of $T_2 = 70$ K they find evidence of PDA state, which is frozen in at $T_1 = 21$ K. They measure a coercive field strength of more than 22 T at 15 K. They find that the PDA is characterized by loss of order within one third of the chains.

Mikhailova et al. found lower values of $T_1 = 15$K [31], but no evidence for an AF state in the neutron diffraction data. They note an AF state cannot be inferred from the Curie-Weiss fitting parameter alone, as temperature-dependent interactions due to SOC may lead to significant deviations from Curie-Weiss behavior. Singleton et al. (2016) found a record coercive field strength of 55 T, and suggest that yet another transition may take place at still higher field strengths [32].

In a single crystal neutron diffraction study, LeFrancois et al. (2014) found a magnetic order aligned with the C_3 rotation axis and ferrimagnetic intra-chain ordering[29]. In another neutron diffraction study, Toth et al. [8]. measured the dispersion and temperature dependence of a magnon between 30 and 38 meV. They compare the results to a generic Dzyaloshinski-Moriya model Hamiltonian and fit the exchange parameters under various global order assumptions. They find that the largest term in the Hamiltonian is the AF exchange between nearest neighbor Ir-Ni sites, with a strong anisotropy on the Nickel site, and a much weaker one on the Ir-site.

5.3 Computational Studies

Following the discovery of SOC-induced Mott states in 5d TMOs, Zhang et al. (2010) undertook a computational study of Sr_3NiIrO_6, using DFT calculation with the Wu and Cohen GGA functional and the inclusion of a Hubbard-U parameter on both the Ni and Ir sites, which wrongly predicted a metallic ground state. The addition of an SOC term on the Ir site, however, opened up a small gap, even when the correlation on the Ir site was decreased to 0.5 eV, and they conclude that it is an SOC-induced Mott insulator. They attribute the AF coupling to an oxygen-mediated superexchange pathway, and describe the ground-state Ir^{4+} configuration as $(t_{2g})e_g^3a_{1g}^2$, i.e. a single hole in the t2g-manifold occupies the $(t_{2g})e_g$-orbital [33].

A similar but spin-polarized calculation was attempted shortly thereafter by another team [34] who failed to stabilize any but an FM groundstate. While they acknowledge that the exchange pathway suggested by Zhang et al. is AF in nature, they propose two additional FM pathways: one O-mediated pathway between the half-filled Ni e_g orbitals and the unoccupied Ir $(e_g)e_g$ orbitals, and a direct one between the Ni and Ir t_{2g}-derived orbitals.

An LSDA+U calculation by Ou and Wu (2014) found an *insulating* FM solution, from both AF and FM initial configurations, whose ground-state is characterized by an A_{1g}-hole in the Ir t_{2g} manifold. The addition of SOC, however, led to an AF state, characterized by a hole in the $(t_{2g})e_g$-manifold [5]. Another computational study by Gordon et al. (2016) stabilized both intrachain FM and AF states, of which the AF state is more stable with at the GGA+U level, and insulating with the inclusion of SOC. They also find that the preferred spin orientation depends on the nature of the exchange coupling, with AF coupling associated with spin orientation parallel to the c-axis, and FM coupling associated with a perpendicular spin orientation. This, they find, is because the AFM groundstate has an a_1g hole due to

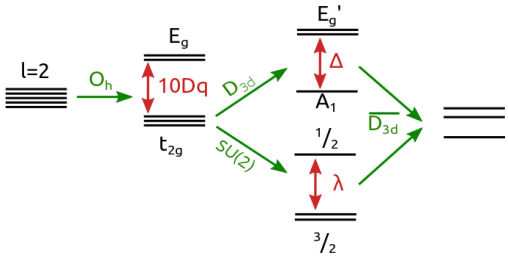

Figure 2: Splitting of the O(3) degeneracy of the Ir-centered d-shell in an IrO_6-cluster by lowering of symmetry to that of the double cover of D_{3d}.

strong interactions with the d-orbitals on the nickel site [6].

5.4 RIXS Spectrum

Lefrancois et al. studied the RIXS spectrum of Sr_3NiIrO_6at the Ir L3-edge [7]. They identify 2 features at 568(3) and 728(5) meV as d-d excitations, and one strongly temperature dependent feature at [55 - 85] meV as a magnonic excitation. Although no visible dispersion was detected, the RIXS spectrum of a spin-wave excitation entangled with a d-d excitation may not have any momentum dependence, as the d-d excitation can act as a momentum sink [35]. A weak feature seen at about 350 meV is noted but has not been identified. They fit the results to a model Hamiltonian for a single hole in the t2g-shell, subject to SOC and a D_3d crystal field, but neglecting any exchange-field terms (figure 2). Of the three possible parametrizations (figure 3a, table 2) they consider only the two with largest value of λ, probably because it is expected to be about 0.3 - 0.4 meV [36]. They find the parametrization with the positive value of Δ, termed here R+, is in better agreement with neutron diffraction data [29], and agrees well with the parameters derived from a multireference configuration interaction study.

6 Methods

6.1 Single electron model

A model Hamiltonian for an electron-hole in the t2g-shell is given in matrix form with respect to a basis of the free tensor product of the three partners a, e_+, and e_- of D_{3d} irreps A_{1g} and E_g with the Pauli spinors $|\pm\rangle$ as

$$\hat{\mathcal{H}} = \sum_{\substack{\gamma\in\{+,-\}\\ s\in\{+,-\}}} \frac{\Delta}{3}(|(E\gamma;s)^*\rangle\langle(E\gamma;s)^*| - |(A;s)^*\rangle\langle(A;s)^*|) + \lambda(L\cdot S)\Big|_{T_{2g}} \tag{40}$$

Where $(L \cdot S)$ is the restriction in both domain and target of the total spin orbit coupling operator to the T_{2g} shell, justified by the quenching of angular momentum by the dominant octahedral field[19, p155]. We compute this using the change of basis

$$\begin{pmatrix} |a\rangle \\ |e_-\rangle \\ |e_+\rangle \end{pmatrix} \to R_d(r) \begin{pmatrix} Y_{2-2}(\theta,\phi) \\ Y_{2-1}(\theta,\phi) \\ Y_{2\ 0}(\theta,\phi) \\ Y_{2\ 1}(\theta,\phi) \\ Y_{2\ 2}(\theta,\phi) \end{pmatrix} \tag{41}$$

given by

$$B_{t_{2g}} = \begin{pmatrix} 0 & 0 & 1 & 0 & 0 \\ -\frac{1}{\sqrt{3}} & -\frac{i}{\sqrt{6}} & 0 & -\frac{i}{\sqrt{6}} & -\frac{1}{\sqrt{3}} \\ -\frac{i}{\sqrt{3}} & -\frac{1}{\sqrt{6}} & 0 & \frac{1}{\sqrt{6}} & \frac{i}{\sqrt{3}} \end{pmatrix} \tag{42}$$

whose action in the adjoint representation on the 1-particle SOC operator gives the restriction

$$\mathbf{l}\cdot\mathbf{s}\Big|_{T_{2g}} = (B_{t_{2g}}\otimes\mathbb{I}_2)^\dagger \mathbf{l}\cdot\mathbf{s}(B_{t_{2g}}\otimes\mathbb{I}_2) \tag{43}$$

and we use the relation $\mathbf{L}\cdot\mathbf{S}\Big|_{T_{2g}}|a^*\rangle = -\mathbf{l}\cdot\mathbf{s}\Big|_{T_{2g}}|a\rangle$ to find its further (endomorphic) restriction to the t_{2g}^5 configuration.

An objective function is given by

$$\chi^2(\Delta,\lambda) = \sum_i \left(\frac{E_i - H}{\sigma_{E_i}}\right)^2 \tag{44}$$

where E_i is the difference from ground state of the observed $d-d$ excitation with uncertainty σ_{E_i}. This resembles the objective function of the least squares method, whose minimization corresponds to the maximization of the likelihood function. Since we have two observed energy differences and the same number of free parameters, we must be able to find a minimum arbitrarily close to zero, and χ^2 has no significance as a test statistic.

We find three roots to this equation, leading to three possible parameterizations of the model Hamiltonian, only two of which were considered in [7]. These are shown in figure 3a. These parameterizations constitute three hypotheses, and are listed in table 2.

For each of the three hypotheses, we solve the Hamiltonian eigenvalue equation, order the eigenstates by energy E_i, $i = 0, \ldots, 6$ and label the corresponding eigenstates $|i\rangle$.

This allows us to then compute the leading contribution to the RIXS cross-section within the dipole approximation as

$$I(E_T;\boldsymbol{\varepsilon}_i,\boldsymbol{\varepsilon}_o) \propto \sum_{(i,f)\in\mathcal{D}(E_T)} P(E_i)\left|\sum_{m_j=-3/2}^{3/2} \frac{\left\langle f\middle|\mathcal{T}_d^\dagger(\varepsilon_o)\middle|m_j^*\right\rangle \left\langle m_j^*\middle|\mathcal{T}_d(\varepsilon_i)\middle|i\right\rangle}{E_T+i\Gamma}\right|^2 \tag{45}$$

where $\mathcal{D}(E_T) = \{(i,f) \in [0,5]^2 \subset \mathbb{Z}^2 | E_f - E_i = E_T\}$, $P(E_i)$ is the probability that a multiplet is initially in the state $|i\rangle$ and $\left|m_j^*\right\rangle$ is the unique state with a hole the $L_{3/2}$ - edge and a fully occupied T_2g-manifold.

The matrix elements decompose into angular and radial integrals, and the latter are identical for all the terms within the employed approximations, and we neglect them entirely. Factoring out the radial part allows us to write any state as a linear combination of tensor products of spherical harmonics with spin functions $|a\rangle = \sum_{m=-l}^{l} \sum_{s\in\{+,-\}} |lm\rangle\,|s\rangle$.

Factoring out the spin functions and writing the vector transition operators in spherical basis leaves us with matrix elements of the form

$$\langle l_1 m_1^* | Y_{1,m}(\theta,\phi) | l_2 m_2^* \rangle$$

which we compute using equation 28 and the relation

$$Y_{l,m}^* = (-1)^m Y_{l,-m} \tag{46}$$

thus reducing each term in the amplitude to a weighted sum over Wigner 3j-symbols.

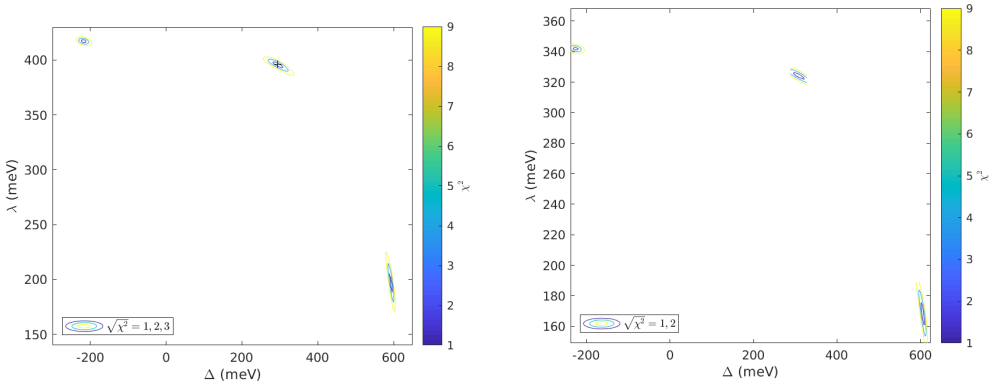

(a) Single-electron (b) Multiplet

Figure 3: Roots to the objective equation. The innermost ellipse indicates the uncertainty in the parameters and their correlation.

This amplitude calculation is written as a suite of MATLAB routines.

At the core of these is `transition_sph(ll,lr,k)` which returns the transition matrix whose elements are

$$T_{ml,mr} = \langle ll, ml* | C_k^{(1)} | lr, mr* \rangle \tag{47}$$

where $C_k^{(1)}$ is the renormalized spherical harmonic and the star indicates conjugation. This function is used by
`kramers_heisenberg_resonant(V,Vn,pin,pout)`
which returns the square of the absolute value of the resonant dipole transition matrix element from each initial state vector in the list `V` to any final state vector in the list, with intermediate states in `Vn`. The thermal average is then taken by the calling routine. The code is hosted by github at
`https://github.com/chnyok/RIXS_Sr3NiIrO6.git`

6.2 Polarization dependence

The dipole transition operators are polarization dependent, and higher order transition operators depend on the wave vectors as well. As the polarization is in the scattering plane, knowledge of the wave vectors suffices to deduce the polarization vectors. The published experiment [7] only reports the momentum transfer $\mathbf{q}$, which fixes 3 of the 4 angular degrees of freedom for the wave vectors, and this leaves one rotational degree of freedom that leaves $\mathbf{q}$

Table 1: Slater Condon parameters from Hartree-Fock calculation

Parameter:	F^2_{dd}	F^4_{dd}	F^4_{pd}	G^1_{pd}	G^3_{pd}
Value:	14.3 eV	9.93 eV	3.27 eV	2.93 eV	1.76 eV

fixed. This parameter is fixed by specifying $\boldsymbol{\sigma}$, the orientation of the scattering plane. The dependence of the scattering amplitudes on $\boldsymbol{\sigma}$, as shall see in the next section, is critical. This parameter was communicated by the authors, and is given (within 0.1%) in hexagonal crystal coordinates as (27 1 -67).

The polarization vector must be described in the same Cartesian basis as the spherical harmonic basis functions $Y_{l,m}(\frac{\mathbf{r}}{r})$ are defined. Since our model Hamiltonian describes an isolated IrO_6 cluster, which has two distinct orientations with respect to the global crystal coordinates, we must take an average of these two orientations. This is more easily accomplished by rotating the polarization vectors than by redefining the orbitals. The C_3 cluster axis coincides with the C_3 crystal axis.

6.3 Full multiplet calculation

The full-multiplet calculation is performed using the Quanty many-body scripting language[37]. This entails a larger number of parameters. The Slater-Condon parameters (table 1) are calculated using radial wavefunctions obtained from a Dirac-Hartree-Fock calculation, employing Cowan's code [38, 39], of the bare Ir^{4+} ion, and are multiplied by a uniform scaling factor $S_{\mathrm{HF}} = 0.8$. An additional Crystal-Field term M_E, governing the configuration mixing of the two E_g levels in the d^1 configuration, occurs, and as initially set to 0 to coincide with its value in the octahedral limit, and later varied.

The crystal-field splitting of a d-shell in a generic field of D_{3d} symmetry is parametrized in terms of the single occupation splitting parameters Δ, Dq and M_E as ($A_{k,m} = \sqrt{\frac{2k+1}{4\pi}} a_{k,m}$)

$$A_{k,m} = \begin{cases} \Delta - 2M_E & k,m = 2,0 \\ -14Dq + \frac{4}{3}\Delta + 2M_E & k,m = 4,0 \\ -i\sqrt{\frac{7}{10}}\left(20Dq + \frac{2}{3}\Delta + M_E\right) & k,m = 4,\pm 3 \end{cases} \tag{48}$$

the spherically symmetric terms $A_{0,0}$ and $F^0_{mm'}$ are neglected, as their only

Table 2: Roots to the objective equation $\chi^2(\Delta, \lambda) = 0$

Hypothesis	Δ_{1e}(meV)	λ_{1e}(meV)	Δ_m(meV)	λ_m(meV)
H_+	294(13)	396(3)	308(13)	324(2)
H_-	−218(4)	417(2)	−225(7)	342(1)
H_3	594(4)	196(9)	606(4)	168(8)

effect is to uniformly shift the barycenter of a shell.

Any such parametrization depends on a particular choice of Cartesian basis in which the spherical harmonic functions are expressed, and is constrained by the desire that $M_E \to 0$ in the octahedral limit. In this basis the C_3 rotational axis coincides with the z-axis, and one of the 3 C_2 rotational-axes coincides with the x-axis. The partners of the T_{2g} irrep are given in terms of the spherical harmonics defined on this basis by equation 42, and the remaining partners of the higher-lying E_g irrep are given similarly by

$$B_{e_g} = \begin{pmatrix} -\frac{i}{\sqrt{6}} & \frac{1}{\sqrt{3}} & 0 & -\frac{1}{\sqrt{3}} & \frac{i}{\sqrt{6}} \\ -\frac{1}{\sqrt{6}} & \frac{i}{\sqrt{3}} & 0 & \frac{i}{\sqrt{3}} & -\frac{1}{\sqrt{6}} \end{pmatrix} \tag{49}$$

We seek roots for the objective function in equation 44. As in the single electron case, there are three of these, and their correspondence is clear. They are listed in table 2. The RIXS cross-section is calculated for each of the resultant parameterizations

6.4 One-electron model within the full multiplet code

Withing the framework of a full multiplet code, the approximations made in our own single electron model can be described by setting the scaling parameter to zero and increasing 10Dq enough to preclude any SOC-induced $e_g - t_{2g}$ orbital mixing. We use this description to test whether the difference between our own code and the full multiplet calculation are attributable to the additional approximations entailed or whether they are a byproduct of small differences in the calculation of broadening effects.

6.5 Temperature dependence parameter extraction

For a quantitative analysis of the temperature dependence of the [55-90] meV feature of the RIXS spectrum, we fit 4 Gaussian functions with parameters

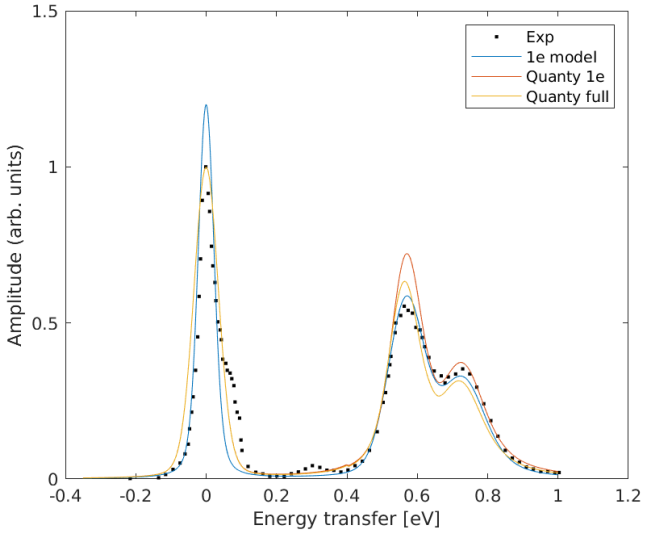

Figure 4: Comparison of one-electron model (blue) with Quanty full multiplet calculation both with (red) and without (green) the one electron approximation for the R1 parametrization.

A_i, σ_i, μ_i to the experimental data. This data is obtained by digitizing graphs from [7], and the error inherent in this process is not included in the error analysis, which accounts only for the covariance in the fitting parameters.

7 Results and discussion

7.1 Comparison with full multiplet calculation

A comparison of the spectral calculation for the parametrization R+ ($a_z = 0$) is shown in figure 4. Both the one-electron model and the full multiplet calculation with the one electron approximation slightly underestimate the elastic peak, since they respectively neglect or suppress the contributions of the e_g orbitals thereto. The effects of e_g - t_{2g} mixing are otherwise apparent only in the difference in the parameters required to reproduce the experimental spectra (table 2). The degree of e_g character in the ground state for the full multiplet calculation for all three parametrizations is shown in table 3.

The computed RIXS spectrum for the three parameterizations with no spin flip term is independent of temperature, as thermal effects enter the model only via the increased occupancy of the first excited state, which is spin

Table 3: e_g - t_{2g} mixing in the ground and first excited states, $\langle N_{e_g} \rangle$

Hypothesis	State	$\alpha_z = 0$	$\alpha_z = 80$ meV	$\alpha_z = 160$ meV
H_+	g	5.9%	5.8%	5.7%
H_+	1		5.9%	6.0%
H_-	g	6.9%	6.2%	6.9%
H_-	1		6.2%	6.2%
H_3	g	4.8%	3.7%	3.7%
H_3	1		3.8%	3.8%

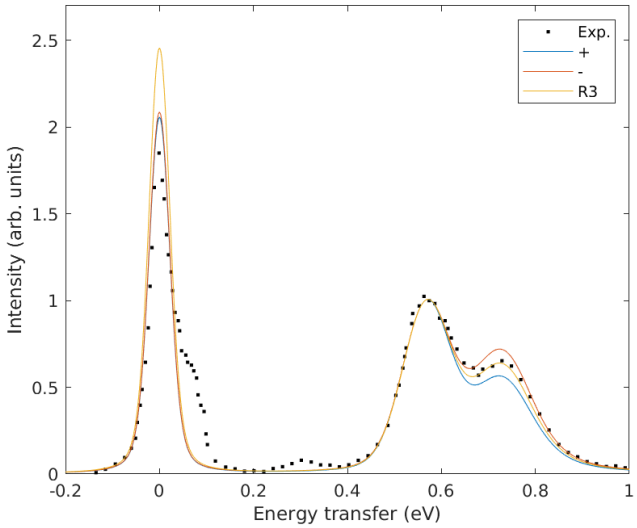

Figure 5: Computed 1e-model RIXS cross-section for three parameterizations sans spin-flip term compared with experimental data at 300 K.

degenerate. These are compared with the room temperature experimental results in figure 5. Although the third parametrization is the most visually appealing, the lack of a quantitative error analysis makes it difficult to draw any conclusions. As the model spectrum consists of delta functions, intrinsic and instrumentation broadening effects are simulated by the convolution of a Gaussian with the Lorentzian distribution. This leaves two free parameters for each peak, which are fit to experiment.

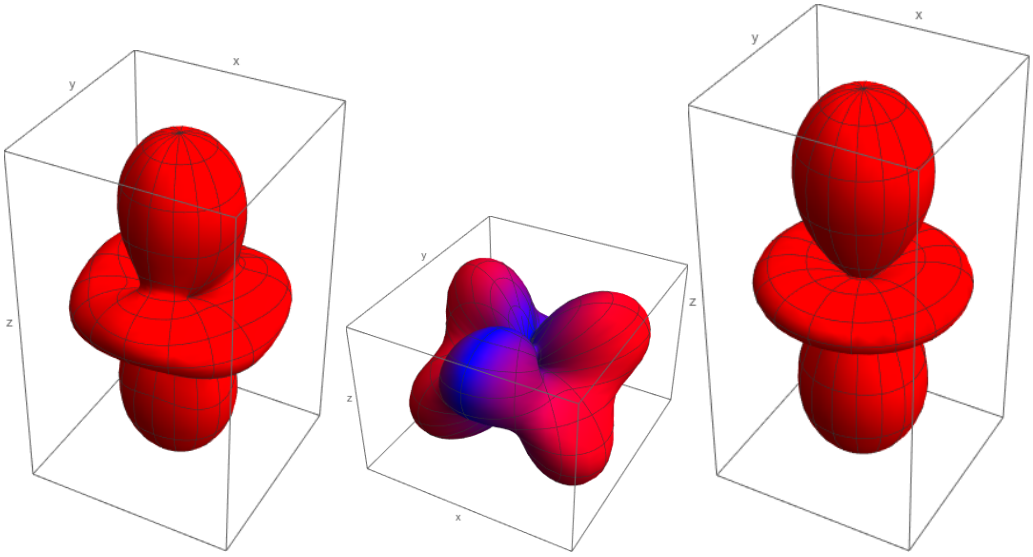

(a) R+ (b) R- (c) R3

Figure 6: Visualization of the hole in the ground state for each of the three spin-free parametrizations of the Hamiltonian.

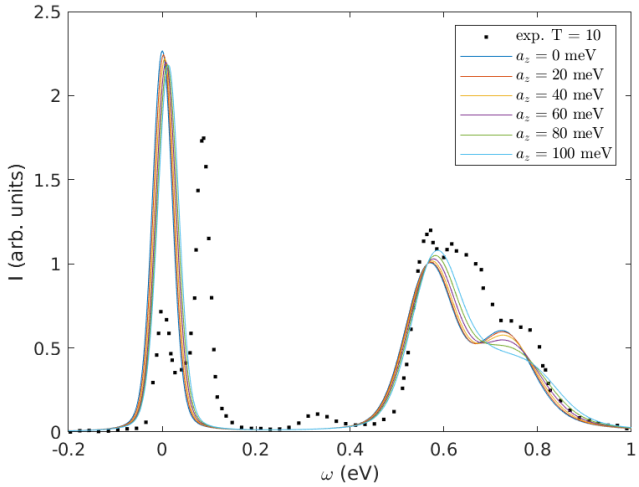

Figure 7: Computed 1e-model RIXS cross-section for R+ parameterization with spin-flip term, compared with experimental data at 10 K.

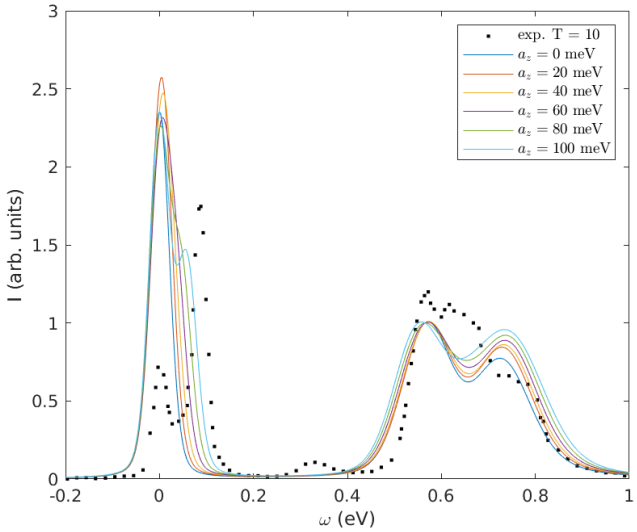

Figure 8: Computed 1e-model RIXS cross-section for R- parameterization with spin-flip term, compared with experimental data at 10 K.

7.2 Effect of the exchange field

The introduction of a local spin-flip term along the C_3-axis splits the degeneracy of all three levels (figures 7 - 12), opening a small gap between

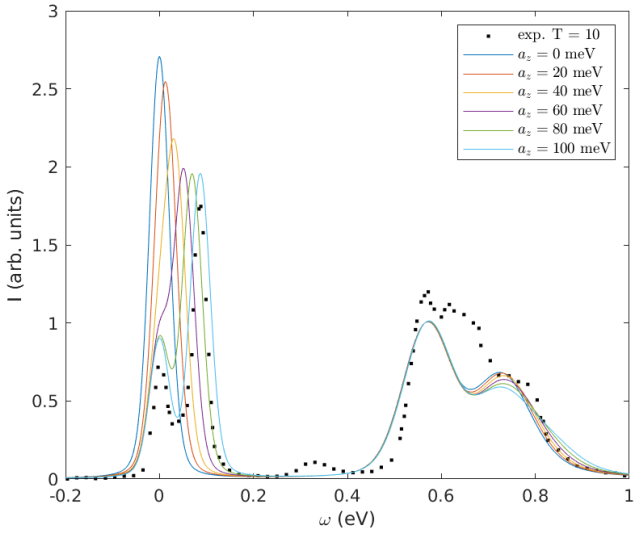

Figure 9: Computed 1e-model RIXS cross-section for R3 parameterization with spin-flip term, compared with experimental data at 10 K.

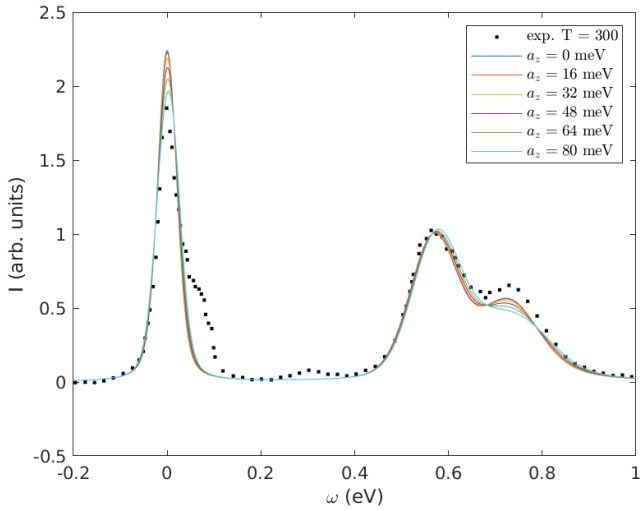

Figure 10: Computed 1e-model RIXS cross-section for R+ parameterization with spin-flip term, compared with experimental data at 300 K.

the highest occupied and lowest unoccupied molecular orbitals. The degree of this splitting differs for the different parameterizations, and is most pronounced in the R3-parameterization, as it has the least spin-orbit coupling.

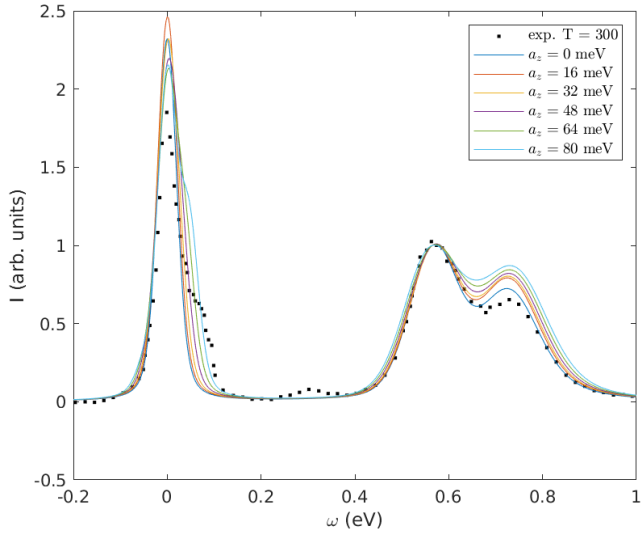

Figure 11: Computed 1e-model RIXS cross-section for R- parameterization with spin-flip term, compared with experimental data at 300 K.

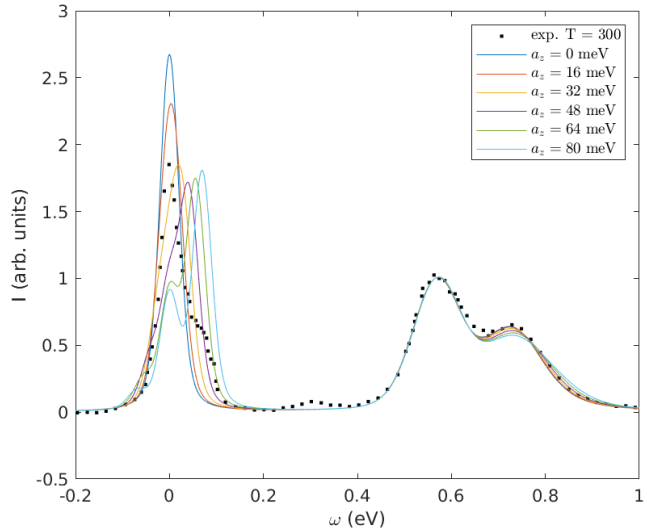

Figure 12: Computed 1e-model RIXS cross-section for R3 parameterization with spin-flip term, compared with experimental data at 300 K.

The entanglement of spin and orbital degrees of freedom leads to an energetic trade-off between a favorable spin alignment and orbital symmetry. This can be visualized by comparing figure 14 with 6. The width of the energy gap opened by the introduction of an exchange field term α_z is largest when the spin and orbital degrees of freedom are completely decoupled. At the other extreme, the R+ parameterization is most strongly coupled, and the polarization of its ground state along this axis is suppressed by the cost of mixing in energetically unfavorable orbitals.

After opening a small gap by splitting the degeneracy, the first excited state has non-negligible occupation even at low temperatures. This means that, in addition to the elastic line, there are 9 Stokes and one anti-Stokes lines in the d-d part of the spectrum. However, depending on the exact parametrization, only 3-5 peaks are resolvable. This is partially due to their proximity, but also some the amplitudes are greatly suppressed by the selection rules in the dipole matrix elements. This effect is most clearly visible in the R3 parametrization, where spectral weight shifts from the elastic line to the first Stokes line.

In figure 9, we see that the addition of a local spin-flip term of about 100 meV is able to reproduce the observed magnonic feature at 10 K. However the effect of this term on the 568 meV and the 728 meV features does not correspond well with observations, and from figure 12 we see that the room tem-

perature spectrum is not well explained by this model. The agreement at 300 K may be improved by including the phonon contribution to the spectrum. This would entail the calculation of all the transition elements $c_i^\dagger \varepsilon \cdot \mathbf{r} c_j$, where $c_i^\dagger(c_i)$ are the phonon creation (annihilation) operators projected onto some suitable local basis. The phonon contribution to the spectrum is responsible for the much of the fine structure visible in low-temperature experiments, and may therefore also explain to some extent the lack of agreement for the higher d-d excitations. An explicit calculation of the phonon contribution would require accurate parameters from quantum chemistry calculations, and are therefore beyond the scope of this work.

7.3 Temperature dependence

The RIXS amplitude of a spin-wave is proportional to the spin-susceptibility [35, 40, 20], which is the magnitude of fluctuations ΔS^2. This may be compared with the dependence on the Debye-Waller factor for scattering from phonons, however no prior knowledge of the temperature-dependence of spin-susceptibility is assumed. The temperature dependence of the magnonic feature is calculated by fitting four Gaussians to the experimental spectra obtained at 10, 20 , 100, 150 and 300 K and comparing the amplitudes of the elastic and first excited states. The results are compared with a phenomenological model function describing Boltzmann-like temperature-dependent dissipation in figure 13.

8 Conclusion and outlook

In this work, the RIXS spectrum of $Sr_3NiIrO_6$was studied at the L3-resonance in the sub-eV energy transfer range, which includes crystal-field and magnetic excitations. An effective one-electron model is developed for this task. The results are compared with the experimental RIXS spectra and to another crystal-field multiplet theory calculation using the software Quanty [37].

The results of this calculation strongly suggest that of the possible one electron model Hamiltonians, the overlooked R3-parametrization best describes the RIXS spectrum of Sr_3NiIrO_6. The temperature-dependent magnetic feature in the observed spectra would then, at least in the low-temperature domain, be better be described as a local spin-flip term rather than a low-dispersion magnonic feature. This agrees with the preponderance of evidence [7, 9, 8] for a positive sign of the D_{3d} crystal-field parameter, but entails a dif-

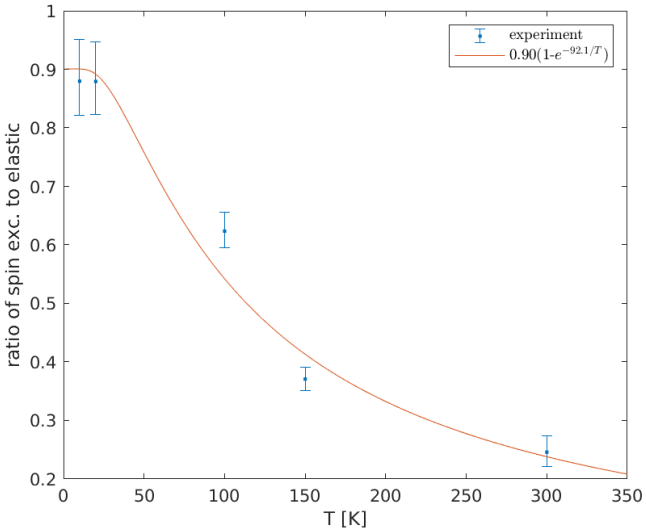

Figure 13: Ratio of low-lying spin excitation to elastic peak as calculated from experiment by Gaussian peak-fitting (blue bars) compared with a phenomenological model (red line).

ferent ratio between it and the spin-orbit coupling parameter. This could be explained by more effective screening of the ground-state hole than is usual, and agrees with the computational studies [33, 5] that found that even a very modest degree of spin-orbit coupling sufficed to predict an insulating ground state.

In conclusion, the methodology developed here yields results in good agreement with experiment and crystal-field multiplet theory. Interestingly, we find that the magnetic excitations observed in the RIXS spectrum can be described as local spin-flip excitations, rather than as dispersive excitations, as has been previously suggested[7]. The agreement with experiment in the low temperature regime can be further improved by treating the entanglement of vibrational modes with the electronic excitation spectra, as for example, in Franck-Condon theory. The drastic reduction of the state space entailed in this one electron model is an initial step that facilitates the creation of an extended model that can be used to model the dispersive excitations and magnetic features of geometrically frustrated $A_3MM'X_6$ compounds.

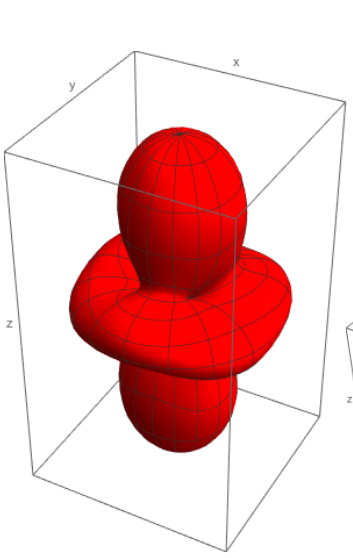

(a) Parametrization 1 ground state

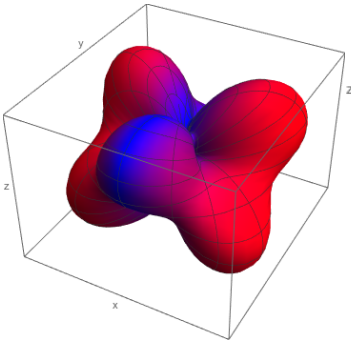

(b) Parametrization 2 ground state

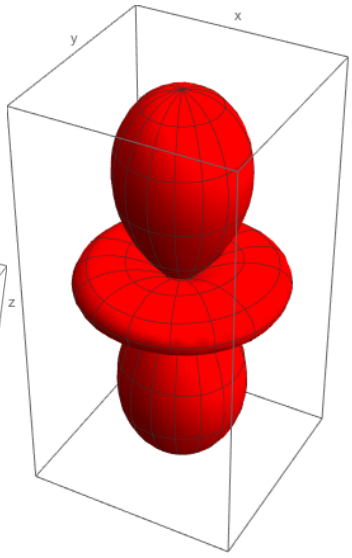

(c) Parametrization 3, ground state

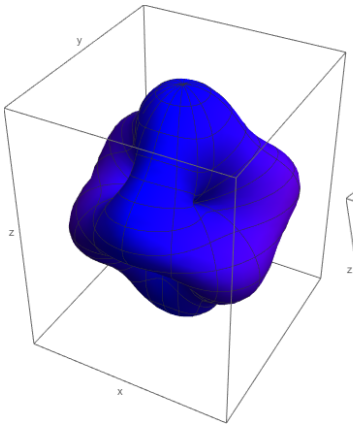

(d) Parametrization 1 First excited state

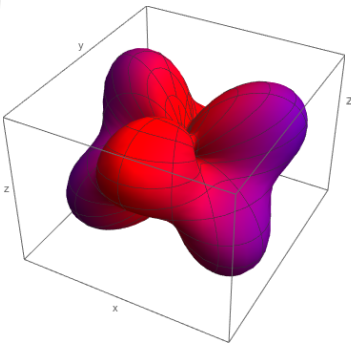

(e) Parametrization 2 First excited state

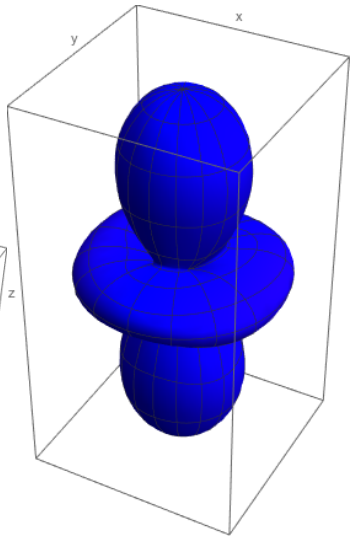

(f) Parametrization 3 First excited state

Figure 14: Visualization of the hole density in the ground state and first excited state for each of the three parametrizations of the Hamiltonian with an exchange field term aligned with the C_3-axis.

References

[1] Jeffrey G. Rau, Eric Kin-Ho Lee, and Hae-Young Kee. "Spin-Orbit Physics Giving Rise to Novel Phases in Correlated Systems: Iridates and Related Materials". In: *Annual Review ofCondensed Matter Physics* (2015). ISSN: 1947-5454. DOI: 10.1146/annurev-conmatphys-031115-011319. arXiv: 1507.06323. URL: http://arxiv.org/abs/1507.06323%7B%5C%%7D0Ahttp://dx.doi.org/10.1146/annurev-conmatphys-031115-011319.

[2] Coch Kim et al. "Square Lattice Iridates". In: *Annual Review ofCondensed Matter Physics* (2018), pp. 315–336. ISSN: 1947-5454. DOI: 10.1146/annurev-conmatphys-031218-013113.

[3] Tôru Moriya. "Anisotropic Superexchange Interaction and Weak Ferromagnetism". In: *Physical Review* 120.1 (Oct. 1960), pp. 91–98. ISSN: 0031-899X. DOI: 10.1103/PhysRev.120.91. URL: https://link.aps.org/doi/10.1103/PhysRev.120.91.

[4] Maria Hermanns, Itamar Kimchi, and Johannes Knolle. "Physics of the Kitaev model: fractionalization, dynamical correlations, and material connections". In: (2017). ISSN: 1947-5454. DOI: 10.1146/annurev-conmatphys-033117-053934. arXiv: 1705.01740. URL: http://arxiv.org/abs/1705.01740%7B%5C%%7D0Ahttp://dx.doi.org/10.1146/annurev-conmatphys-033117-053934.

[5] Xuedong Ou and Hua Wu. "Impact of spin-orbit coupling on the magnetism of Sr 3 MIrO 6 (M = Ni, Co)". In: *Scientific Reports* 4 (2014), pp. 1–5. ISSN: 20452322. DOI: 10.1038/srep04609. arXiv: arXiv:1312.7411v1.

[6] Elijah E. Gordon et al. "Spin orientations of the spin-half Ir4+ions in Sr3NiIrO6, Sr2IrO4, and Na2IrO3: Density functional, perturbation theory, and Madelung potential analyses". In: *Journal of Chemical Physics* 144.11 (2016). ISSN: 00219606. DOI: 10.1063/1.4943889. arXiv: 1603.00523.

[7] E. Lefran çois et al. "Anisotropic interactions opposing magnetocrystalline anisotropy in Sr_3NiIrO_6". In: *Phys. Rev. B* 93 (22 June 2016), p. 224401. DOI: 10.1103/PhysRevB.93.224401. URL: https://link.aps.org/doi/10.1103/PhysRevB.93.224401.

[8] S. Toth et al. "Frustrated Ising chains on the triangular lattice in Sr_3NiIrO_6". In: *Phys. Rev. B* 93 (17 May 2016), p. 174422. DOI: 10.1103/PhysRevB.93.174422. URL: https://link.aps.org/doi/10.1103/PhysRevB.93.174422.

[9] Turan Birol, Kristjan Haule, and David Vanderbilt. "Nature of the magnetic interactions in Sr3NiIrO6". In: *Physical Review B* 98.13 (2018). ISSN: 24699969. DOI: 10.1103/PhysRevB.98.134432. arXiv: 1805.03733.

[10] Jean-Louis Heully et al. "Diagonalisation of the Dirac Hamiltonian as a basis for a relativistic many-body procedure Diagonalisation of the Dirac Hamiltonian as a basis for a relativistic many-body procedure". In: *Journal of Physics B* Iii (1986), pp. 2799–2815.

[11] Pekka Pyykko and Jean Paul Desclaux. "Relativity and the Periodic System of Elements". In: *Accounts of Chemical Research* 12.8 (1979), pp. 276–281. ISSN: 15204898. DOI: 10.1021/ar50140a002.

[12] L.I. Schiff. *Quantum Mechanics*. International series in pure and applied physics. McGraw-Hill, 1955. URL: https://books.google.fi/books?id=7ApRAAAAMAAJ.

[13] P. Woit. *Quantum Theory, Groups and Representations: An Introduction*. Springer International Publishing, 2017. ISBN: 9783319646121.

[14] Rubin H Laundau. *Quantum Mechanics II*. New York: Wiley, 1990.

[15] E.P. Wigner and J.J. Griffin. *Group Theory and Its Application to the Quantum Mechanics of Atomic Spectra*. Pure and applied Physics. Academic Press, 1959. URL: https://books.google.fi/books?id=IOJEAAAAIAAJ.

[16] H.F. Jones. *Groups, Representations and Physics*. CRC Press, 1998. ISBN: 9781420050295. URL: https://books.google.fi/books?id=OvNp8Df5XukC.

[17] Antoine Georges, Luca de' Medici, and Jernej Mravlje. "Strong Correlations from Hund's Coupling". In: *Annual Review of Condensed Matter Physics* 4.1 (2013), pp. 137–178. DOI: 10.1146/annurev-conmatphys-020911-125045. URL: https://doi.org/10.1146/annurev-conmatphys-020911-125045.

[18] I. Dzyaloshinsky. "A thermodynamic theory of "weak" ferromagnetism of antiferromagnetics". In: *Journal of Physics and Chemistry of Solids* 4.4 (Jan. 1958), pp. 241–255. ISSN: 0022-3697. DOI: 10.1016/0022-3697(58)90076-3. URL: https://www.sciencedirect.com/science/article/pii/0022369758900763?via%7B%5C%%7D3Dihub.

[19] Satoru Sugano, Yukito Tanabe, and Hiroshi Kamimura. *Multiplets of transition-metal ions in crystals*. Academic Press New York, 1970.

[20] Luuk J. P. Ament et al. "Resonant inelastic x-ray scattering studies of elementary excitations". In: *Rev. Mod. Phys.* 83 (2 June 2011), pp. 705–767. DOI: 10.1103/RevModPhys.83.705. URL: https://link.aps.org/doi/10.1103/RevModPhys.83.705.

[21] Winfried Schülke. *Electron dynamics by inelastic X-ray scattering*. eng. Oxford series on synchrotron radiation ; 7. Oxford ; New York: Oxford University Press, 2007. ISBN: 1281160067.

[22] P. W. Anderson. "Infrared Catastrophe in Fermi Gases with Local Scattering Potentials". In: *Phys. Rev. Lett.* 18 (24 June 1967), pp. 1049–1051. DOI: 10.1103/PhysRevLett.18.1049. URL: https://link.aps.org/doi/10.1103/PhysRevLett.18.1049.

[23] Michael Knap et al. "Time-Dependent Impurity in Ultracold Fermions: Orthogonality Catastrophe and Beyond". In: *Phys. Rev. X* 2 (4 Dec. 2012), p. 041020. DOI: 10.1103/PhysRevX.2.041020. URL: https://link.aps.org/doi/10.1103/PhysRevX.2.041020.

[24] Cyril Proust and Louis Taillefer. "The remarkable underlying ground states of cuprate superconductors". In: *Annual Review ofCondensed Matter Physics* (2018), pp. 409–429. DOI: 10.1146/((please. arXiv: 1807.05074. URL: http://arxiv.org/abs/1807.05074.

[25] Rui Wang et al. "A Review of Perovskites Solar Cell Stability". In: *Advanced Functional Materials* 1808843 (2019), pp. 1–25. ISSN: 16163028. DOI: 10.1002/adfm.201808843.

[26] Koichi Momma and Fujio Izumi. "{\it VESTA}: a three-dimensional visualization system for electronic and structural analysis". In: *Journal of Applied Crystallography* 41.3 (June 2008), pp. 653–658. DOI: 10.1107/S0021889808012016. URL: https://doi.org/10.1107/S0021889808012016.

[27] Leon Balents. "Spin liquids in frustrated magnets". In: *Nature* 464 (Mar. 2010), 199 EP -. URL: https://doi.org/10.1038/nature08917.

[28] D. Flahaut et al. "A magnetic study of the one dimensional Sr_3NiIrO_6 compound". In: *The European Physical Journal B - Condensed Matter and Complex Systems* 35.3 (Oct. 2003), pp. 317–323. ISSN: 1434-6036. DOI: 10.1140/epjb/e2003-00283-3. URL: https://doi.org/10.1140/epjb/e2003-00283-3.

[29] E. Lefran çois et al. "Magnetic order in the frustrated Ising-like chain compound Sr_3NiIrO_6". In: *Phys. Rev. B* 90 (1 July 2014), p. 014408. DOI: 10.1103/PhysRevB.90.014408. URL: https://link.aps.org/doi/10.1103/PhysRevB.90.014408.

[30] T. N. Nguyen and H. C. zur Loye. "A family of one-dimensional oxides: Sr_3MIrO_6 (M = Ni, Cu, Zn): Structure and magnetic properties". In: *Journal of Solid State Chemistry* 117.2 (1995), pp. 300–308. ISSN: 1095726X. DOI: 10.1006/jssc.1995.1277.

[31] D. Mikhailova et al. "Magnetic properties and crystal structure of Sr_3CoIrO_6 and Sr_3NiIrO_6". In: *Phys. Rev. B* 86 (13 Oct. 2012), p. 134409. DOI: 10.1103/PhysRevB.86.134409. URL: https://link.aps.org/doi/10.1103/PhysRevB.86.134409.

[32] John Singleton et al. "Magnetic properties of Sr3NiIrO6 and Sr3CoIrO6: Magnetic hysteresis with coercive fields of up to 55 T". In: *Physical Review B* 94.22 (2016), pp. 4–13. ISSN: 24699969. DOI: 10.1103/PhysRevB.94.224408.

[33] G. R. Zhang et al. "Intrachain antiferromagnetic interaction and Mott state induced by spin-orbit coupling in Sr3NiIrO6". In: *Journal of Applied Physics* 107.9 (May 2010), 09E120. ISSN: 0021-8979. DOI: 10.1063/1.3360339. URL: http://aip.scitation.org/doi/10.1063/1.3360339.

[34] Soumyajit Sarkar, Sudipta Kanungo, and T. Saha-Dasgupta. "Ab initio study of low-dimensional quantum spin systems Sr_3NiPtO_6, Sr_3CuPtO_6, and Sr_3NiIrO_6". In: *Phys. Rev. B* 82 (23 Dec. 2010), p. 235122. DOI: 10.1103/PhysRevB.82.235122. URL: https://link.aps.org/doi/10.1103/PhysRevB.82.235122.

[35] M. W. Haverkort. "Theory of Resonant Inelastic X-ray Scattering by Collective Magnetic Excitations". In: (Nov. 2009). DOI: 10.1103/PhysRevLett.105.167404. arXiv: 0911.0706. URL: http://arxiv.org/abs/0911.0706%20http://dx.doi.org/10.1103/PhysRevLett.105.167404.

[36] A. E. Taylor et al. "Spin-Orbit Coupling Controlled J=3 /2 Electronic Ground State in 5d3 Oxides". In: *Physical Review Letters* 118.20 (2017), pp. 1–6. ISSN: 10797114. DOI: 10.1103/PhysRevLett.118.207202.

[37] M. W. Haverkort, M. Zwierzycki, and O. K. Andersen. "Multiplet ligand-field theory using Wannier orbitals". In: *Phys. Rev. B* 85 (16 Apr. 2012), p. 165113. DOI: 10.1103/PhysRevB.85.165113. URL: https://link.aps.org/doi/10.1103/PhysRevB.85.165113.

[38] Robert D. Cowan and Donald C. Griffin. "Approximate relativistic corrections to atomic radial wave functions*". In: *J. Opt. Soc. Am.* 66.10 (Oct. 1976), pp. 1010–1014. DOI: 10.1364/JOSA.66.001010. URL:

http://www.osapublishing.org/abstract.cfm?URI=josa-66-10-1010.

[39] Robert Duane Cowan. *The theory of atomic structure and spectra*. Univ. of California, 2001. ISBN: 0520038215,9780520038219.

[40] Luuk J. P. Ament et al. "Theoretical Demonstration of How the Dispersion of Magnetic Excitations in Cuprate Compounds can be Determined Using Resonant Inelastic X-Ray Scattering". In: *Physical Review Letters* 103.11 (Sept. 2009), p. 117003. ISSN: 0031-9007. DOI: 10.1103/PhysRevLett.103.117003. URL: https://link.aps.org/doi/10.1103/PhysRevLett.103.117003.